Available online at www.sciencedirect.com
ScienceDirect
Journal of Sound and Vibration 324 (2009) 221–242
JOURNAL OF SOUND AND VIBRATION
www.elsevier.com/locate/jsvi

# A receptance harmonic balance technique for the computation of the vibration of a whole aero-engine model with nonlinear bearings

Philip Bonello*, Pham Minh Hai

*School of Mechanical, Aerospace and Civil Engineering, University of Manchester, UK*

Received 28 July 2008; received in revised form 24 November 2008; accepted 22 January 2009
Handling Editor: C.L. Morfey
Available online 3 March 2009

**Abstract**

Current frequency-domain techniques for the rapid computation of the steady-state periodic vibration of unbalanced rotordynamic systems with nonlinear bearings are not suitable for realistic engine structures like aero-engine assemblies. In this paper, a whole-engine receptance harmonic balance method (RHBM) is devised that, for the first time, allows the frequency domain analysis of such a structure. The method uses the receptance functions of the linear part of the structure under non-rotational conditions, obtained from a one-off eigenvalue analysis, to set up the equations for the rotating nonlinear assembly. The unknowns solved for are the Fourier coefficients of the relative displacements at the nonlinear bearings plus a few extra unknowns. These latter unknowns enable solution of the problem in the presence of statically indeterminate rotors that have just one linear point support or none at all. Simulation tests on a realistically sized representative twin-spool engine showed excellent correlation with time-marching results obtained from the recently developed impulsive receptance method (IRM). It is demonstrated that, when used in conjunction with a time-marching solver like the IRM, the RHBM is a very powerful tool that should greatly facilitate the hitherto highly restricted nonlinear dynamic analysis of realistic engine structures.


## 1. Introduction

Aero-engine assemblies are complex structures typically involving at least two nested rotors mounted within a flexible casing via squeeze-film damper (SFD) bearings. Most SFDs are unsupported, as can be seen in Fig. 1, where a parallel retainer spring is only used with one SFD at the end of each rotor. As observed in Ref. [1], the deployment of SFDs into such structures is highly cost-effective but requires careful calculation since they can be highly nonlinear in their performance.

The solution techniques for the response of a nonlinear system subjected to periodic external excitation (e.g. rotor unbalance) can be broadly categorised into either time domain or frequency domain techniques. Time domain (''time-marching'') techniques march forward in time past the initial transient stage to yield the

*Corresponding author.
*E-mail address:* philip.bonello@manchester.ac.uk (P. Bonello).

0022-460X/$ - see front matter © 2009 Elsevier Ltd. All rights reserved.
doi:10.1016/j.jsv.2009.01.039

**Nomenclature**

$()^{\mathrm{T}}$ matrix/vector transpose

$[\dot{\ }]$ d$()$/d$t$

$\overline{()}, ()^{(k)}_{\cos}, ()^{(k)}_{\sin}$ Fourier coefficients of vector $()$, e.g. Eq. (3)

$\mathbf{A}_{\mathbf{J}_{\mathrm{sel}}\mathbf{v}}(\omega), \mathbf{A}_{\mathbf{J}_{\mathrm{sel}}\mathbf{w}}(\omega)$ accelerance matrices, Eqs. (27a) and (27b)

$\mathbf{B}(k\varpi)$ matrix, Eq. (23b)

$\mathbf{C}_{\mathbf{JJ}}(\omega), \mathbf{C}_{\mathbf{vv}}(\omega), \ldots\ldots$ receptance matrices

$\tilde{\mathbf{C}}_{\mathbf{vv}}(\omega), \tilde{\mathbf{C}}_{\mathbf{vw}}(\omega)$ "incomplete" receptance matrices, Eqs. (33a) and (33b)

$\mathbf{D}(k\varpi), \mathbf{E}(k\varpi), \mathbf{F}(k\varpi)$ matrices, Eqs. (23a) and (25a)

$\mathbf{g}$ $= [\mathbf{g}^{\mathrm{T}}_{(1)} \ \cdots \ \mathbf{g}^{\mathrm{T}}_{(J)}]^{\mathrm{T}}$

$\mathbf{g}_{(j)}$ $= [\mathbf{M}_{(j)1} \ \mathbf{N}_{(j)1} \ \cdots \ \mathbf{M}_{(j)G_J} \ \mathbf{N}_{(j)G_J}]^{\mathrm{T}}$

$Gj$ total number of gyroscopic locations on rotor no. $j$

$\check{\mathbf{H}}_{\mathbf{v}}, \check{\mathbf{H}}_{\mathbf{v}}, \check{\mathbf{H}}_{\mathbf{w}}$ "incomplete" modal matrices defined by Eqs. (32), (40b) and (40c)

$i$ counter for nonlinear bearings

$\mathbf{I}$ identity matrix

$I_{(j)p}$ polar moment of inertia at gyroscopic location no. $p$ of rotor no. $j$

$j$ counter for rotors

$J$ total number of rotors

$k$ counter for harmonics

$K$ maximum of $k$

$\mathbf{L}_{(j)}$ matrix defined by Eq. (25c)

$M_{(j)p}$, $N_{(j)p}$ gyroscopic moments about $x$ and $y$ axes, respectively, at gyroscopic location no. $p$ of rotor no. $j$

$n_{\mathrm{extra}}$ number of extra unknowns ($\bar{\tilde{\mathbf{q}}}$)

$n_F$ number of points of SFD force time history (Fig. 3)

$N$ number of SFDs

$p$ counter for gyroscopic effect location on rotor no. $j$

$P$ total number of rigid body modes

$\mathbf{P}$ block diagonal matrix of diagonal submatrices $\mathbf{P}_{(j)}$, $j = 1 \ldots J$

$\mathbf{P}_{(j)}$ $= \Omega_{(j)}\mathbf{diag}\{-I_{(j)1}, I_{(j)1}, \ldots, -I_{(j)G_j}, I_{(j)G_j}\}$

$\mathbf{q}$ vector of modal coordinates (Eq. (29))

$\bar{\tilde{\mathbf{q}}}, \bar{\tilde{\mathbf{q}}}$ rigid and flexible mode subvectors of $\bar{\mathbf{q}}$ (Eq. (30))

$Q$ positive integer (Eq. (1))

$\mathbf{Q}_{(j)}(k\varpi)$ matrix defined by Eq. (25c)

$r$ counter for modes

$R$ total number of modes considered

$s$ counter for unbalance location on rotor no. $j$

$S_j$ maximum of $s$

$t$ time (s)

$\mathbf{u}_{(j)}$ unbalance excitation vector Eq. (9)

$\mathbf{u}_{(j)\cos}, \mathbf{u}_{(j)\sin}$ component amplitudes of $\mathbf{u}_{(j)}$ Eqs. (10a) and (10b)

$U_{(j)s}$ unbalance at location $s$ on rotor no. $j$ (kg m)

$\mathbf{v}$ $= \mathbf{x}_{\mathbf{J}} - \mathbf{x}_{\mathbf{B}} = [\mathbf{v}^{\mathrm{T}}_1 \ \cdots \ \mathbf{v}^{\mathrm{T}}_N]^{\mathrm{T}}$

$\mathbf{v}_i$ $= [x_{\mathrm{J}_i} - x_{\mathrm{B}_i} \ \ y_{\mathrm{J}_i} - y_{\mathrm{B}_i}]^{\mathrm{T}}$

$\mathbf{v}_{\mathbf{s}}$ vector of static Cartesian offsets at squeeze-film no. $i$ (Eq. (34))

$\mathbf{w}$ static loading distribution vector (all rotors)

$x, y, z$ Cartesian frame, Fig. 1

$x_{\mathrm{B}_i}, y_{\mathrm{B}_i}, x_{\mathrm{J}_i}, y_{\mathrm{J}_i}$ instantaneous Cartesian displacements of the journal and housing centres $\mathrm{J}_i$, $\mathrm{B}_i$ at SFD no. $i$

$\mathbf{x}_{\mathbf{J}}$, $\mathbf{x}_{\mathbf{B}}$ $= [x_{\mathrm{J}_1} \ y_{\mathrm{J}_1} \cdots x_{\mathrm{J}_N} \ y_{\mathrm{J}_N}]^{\mathrm{T}}$, $[x_{\mathrm{B}_1} \ y_{\mathrm{B}_1} \cdots x_{\mathrm{B}_N} \ y_{\mathrm{B}_N}]^{\mathrm{T}}$

$\mathbf{z}$ vector of unknowns (Eq. (35))

$\mathbf{z}_0$ initial approximation for $\mathbf{z}$

$\alpha_{(j)p}, \beta_{(j)p}$ rotational deformation about $x$, $y$ axes, respectively, at gyroscopic location no. $p$ of rotor no. $j$

$\gamma_{(j)s}$ angle defined in text (below Eqs. (10a) and (10b))

$\delta_{k\varpi,\Omega_{(j)}} = \begin{cases} 1, & k\varpi = \Omega_{(j)} \\ 0, & k\varpi \neq \Omega_{(j)} \end{cases}$

$\boldsymbol{\theta}$ $= [\boldsymbol{\theta}^{\mathrm{T}}_{(1)} \cdots \boldsymbol{\theta}^{\mathrm{T}}_{(J)}]^{\mathrm{T}}$

$\boldsymbol{\theta}_{(j)}$ $= [\beta_{(j)1} \ \alpha_{(j)1} \cdots \beta_{(j)G_j} \ \alpha_{(j)G_j}]^{\mathrm{T}}$

$\boldsymbol{\Lambda}, \tilde{\boldsymbol{\Lambda}}$ diagonal matrices, Eqs. (38) and (40a)

$\varpi$ fundamental circular frequency of the RHBM (Eq. (1))

$\bar{\boldsymbol{\rho}}, \boldsymbol{\rho}^{(k)}_{\cos}, \boldsymbol{\rho}^{(k)}_{\sin}$ vectors of Fourier coefficients of all SFD forces (Eqs. (8a)–(8c))

$\boldsymbol{\rho}_i$ $= [Q_{x_i} \ \ Q_{y_i}]^{\mathrm{T}}$ (Cartesian forces on journal at squeeze-film no. $i$)

$\phi_{(j)}$ angle defined in text (below Eqs. (10a) and (10b))

$\boldsymbol{\chi}$ vector function of $\mathbf{z}$, $\Omega_{(j_{\mathrm{ref}})}$ and $Q$ (Eq. (36))

$\boldsymbol{\psi}^{(r)}_{\mathbf{J}}, \boldsymbol{\psi}^{(r)}_{\mathbf{B}}$ mass-normalised eigenvectors defining the $x$ and $y$ displacements of the squeeze-film terminals $\mathrm{J}_i$, $\mathrm{B}_i$ in mode no. $r$

$\boldsymbol{\psi}^{(r)}_{\mathbf{v}}$ $= \boldsymbol{\psi}^{(r)}_{\mathbf{J}} - \boldsymbol{\psi}^{(r)}_{\mathbf{B}}$

$\boldsymbol{\psi}^{(r)}_{\mathbf{J}_{\mathrm{sel}}}$ sub-vector of $\boldsymbol{\psi}^{(r)}_{\mathbf{J}}$ for selected journals (Section 2.3)

$\boldsymbol{\psi}^{(r)}_{\mathbf{u}_{(j)}}, \boldsymbol{\psi}^{(r)}_{\mathbf{g}}, \boldsymbol{\psi}^{(r)}_{\mathbf{w}}$ mass-normalised eigenvectors evaluated at degrees of freedom corresponding to directions and locations of elements in $\mathbf{u}_{(j)}$, $\mathbf{g}$, and $\mathbf{w}$

$\boldsymbol{\psi}^{(r)}_{\boldsymbol{\theta}}$ mass-normalised eigenvectors evaluated at degrees of freedom in $\boldsymbol{\theta}$

$\omega$ generic circular frequency

$\omega_r$ natural frequency of mode no. $r$

$\Omega_{(j)}$ rotational speed of rotor no. $j$ (rad/s)

$\Omega_{(j_{\text{ref}})}$ reference unbalanced shaft speed (Eq. (1))

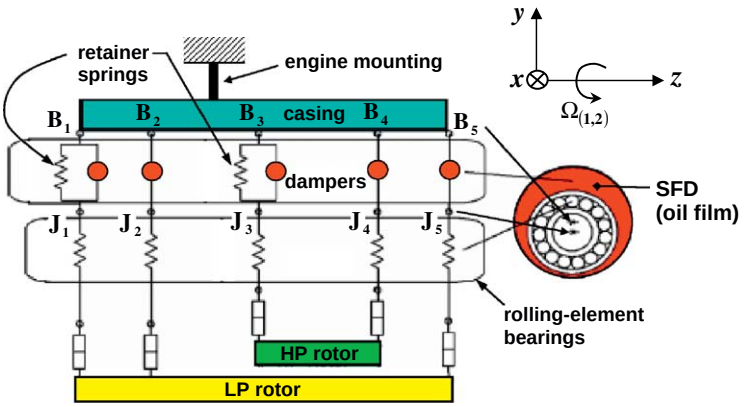


Fig. 1. Schematic of a representative twin-spool engine (abbreviations "LP" and "HP" stand for "low pressure" and "high pressure" respectively).

steady-state response, which may not necessarily be periodic. Frequency domain ("periodic solution") techniques, which employ analytical methods like harmonic balance [2–4] or trigonometric collocation [5], are inherently very much faster since they directly yield steady-state solutions that are assumed to be periodic at an assumed fundamental frequency. However, such periodic vibration may not always be physically possible, in which case the computed periodic solutions represent a dynamic state that is unstable to the slightest physical perturbation. Time-marching is then used to obtain the actual (stable) vibration. An efficient computational facility takes advantage of the relative merits of both categories through an integrated approach that makes effective use of both [6]. This paper will focus on the frequency domain approach.

The direct study of real engine structures has been hindered by the fact that the various frequency-domain techniques proposed for the computation of the unbalance vibration are not suitable for complex systems. Indeed, such methods are almost invariably illustrated on simple rotor-bearing systems e.g. Refs. [2–7]. Moreover, commercial finite-element (FE) codes do not possess a frequency domain solver for nonlinear whole-engine modelling.

The common strategy of all proposed frequency domain techniques for the analysis of rotating systems with concentrated nonlinearities like fluid bearings is to consider the forces from these elements as external to the remaining linear part. What is ultimately solved is a set of nonlinear algebraic equations whose unknowns are the Fourier coefficients of the degrees of freedom at the nonlinearities only. The difference between the various frequency domain techniques lies mainly in the way these equations are generated. Such techniques can then be classified as follows: (a) transfer matrix approach e.g. Ref. [2]; (b) direct FE approach e.g. Refs. [3,4]; (c) direct modal approach [5]; and (d) receptance harmonic balance approach [6,7]. The transfer matrix approach is not suited for modelling complex sub-systems such as the engine casing. The direct FE approach applies the harmonic balance or trigonometric collocation method to the full FE equations of the system. A condensation technique, involving the inversion of large matrices, can then be applied to reduce the number of unknowns to those associated only with the nonlinear degrees of freedom. Such a process is not feasible for a whole-engine model. As stated in Ref. [5], approach (c) is more tractable to large systems since it uses component mode synthesis. However, this requires the prior solution of the eigenproblem of the *rotating* linear part and modal truncation. The latter has been shown in Ref. [1] to be a problem with a real engine due to a

high modal density at relatively low frequencies. Moreover, gyroscopic effects would necessitate the solution of the eigenproblem for *each* speed.

The receptance harmonic balance method (RHBM), as presented in Refs. [6,7], shows great potential for the analysis of complex structures. The nonlinear algebraic equations are yielded without the need of any costly condensation, by applying the force–displacement relationships for each harmonic of the vibration using the frequency response functions (receptances) of the linear part. There is no problem with modal truncation since any desired number of modes can be included in the receptance expressions. This concept was first introduced by Ren and Beards [8] for a simple non-rotating structure. The RHBM was adapted by Bonello et al. [6,7] for a rotating system comprising a single shaft with negligible gyroscopic effect running on nonlinear bearings housed within a flexible support structure. Among the issues considered in Refs. [6,7] was the question of how to derive the equations for the zero-frequency harmonic (i.e. the mean component of the vibration) when the presence of rigid body modes of the linear part cause the relevant receptance functions to be undefined at zero-frequency. Two common examples of this case are: a rotor pivoted at one end by a self-aligning rolling-element bearing and running on an unsupported SFD at the other end [6]; or a rotor running only on two unsupported SFDs [7]. The linear part of the system then comprises a pinned-free rotor in the former case, and a free–free rotor in the latter case. The solution provided in Refs. [6,7] was to consider the fact that the mean components of both velocity and acceleration of the vibration of the nonlinear system are zero. Hence, at zero-frequency such a rotor is in a state of "pseudo-static" equilibrium under the action of the static external forces and the mean SFD forces. The term "pseudo" is used here since the latter forces are themselves generated by the vibration. The works in Refs. [6,7] then proceeded to solve for the vibration response of a *statically determinate* rotor with unsupported SFDs by including the pseudo-static equilibrium equations with the rest of the dynamic frequency response equations.

If the work in Refs. [6,7] is to be used as the basis for solving the unbalance response of a whole aero-engine model the following outstanding issues need to be resolved:

- The presence of rotors that introduce rigid body modes in the linear part but are statically *indeterminate* when the nonlinear bearings are in place: this is clearly the case for the low-pressure (LP) spool in Fig. 1, where the rigid body modes define pivoting motion about $J_1$.
- Gyroscopic effects: for the receptance approach to be feasible, the receptances should pertain to the linear part under non-rotational conditions, making them independent of rotational speed, allowing a one-off analysis of the linear part. Hence, a means has to be found of including gyroscopic effects into the nonlinear problem without adding to the number of unknowns.
- An efficient post-solution recovery of the full set of degrees of freedom.
- Unbalance excitation from more than one rotor: for single shaft systems the external excitation (unbalance) is at a single frequency—single-frequency unbalance (SFU). This also applies for multi-spool systems where the unbalance distribution is confined to only one of the shafts. Frequency domain techniques have so far been used only on SFU problems. In practice, the unbalance may be located on more than one rotor and the unbalanced rotors will turn at different speeds, resulting in multi-frequency unbalance (MFU). It is clearly desirable for the method to be able to handle MFU conditions.

The work presented in this paper resolves the above-mentioned issues. In addition, it reduces the number of unknowns by about half that in previous research by formulating the equations in terms of the *relative* rather than the absolute degrees of freedom at the nonlinearities. This is possible since the inertia of the fluid films at the bearings is commonly assumed to be negligible (e.g. Refs. [1–7]—indeed this assumption appears to be essential in cases where both journal and bearing housing vibrate).

This work is the second stage of a project whose overall aim is to deliver a suite of computational techniques for unbalance response computation, suitable for generic whole-engine models, which will significantly extend the capability of current FE packages. The proposed analysis of the nonlinear rotating assembly uses the modal parameters of the undamped linear part of the assembly under non-rotating conditions (see Fig. 2). Nastran® is used for the linear pre-processing and specially written Matlab® routines for the subsequent nonlinear computation which has both time domain and frequency domain options. The first stage of the project has produced a novel fast time domain technique called the impulsive receptance method (IRM) [1].

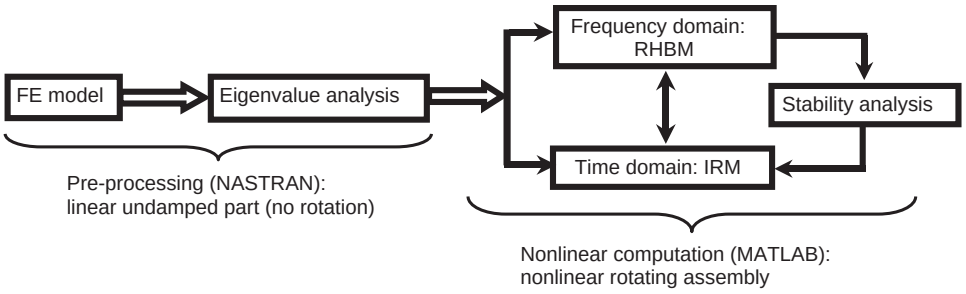


Fig. 2. Overall computational procedure.

The present paper deals with the development of a whole-engine RHBM. The development of a fast stability-check routine for the RHBM solutions will be the subject of a separate paper.

The theory of whole-engine RHBM is presented in the following section. In Section 3 the method is tested on a realistically sized representative twin-spool aero-engine model and validated against the IRM.

## 2. Theory

### 2.1. System description

The modal parameters in all the theory pertain to the linear part of the assembly under non-rotating conditions. By "linear part" is meant the structure that remains in Fig. 1 when the SFDs are replaced by gaps. The damping in the linear part of an engine is commonly regarded as negligible [6]. The linear part is acted on by the SFD forces, unbalance forces, static loading on the rotors, and the gyroscopic moments on the rotors. The engine is assumed to have $J$ rotors each with speeds $\Omega_{(j)}$, $j = 1 \ldots J$.

In the RHBM, the vibration is assumed to be periodic with a fundamental frequency of $\varpi$ where

$$\varpi = \Omega_{(j_{\text{ref}})}/Q. \tag{1}$$

$Q$ is a positive integer and $\Omega_{(j_{\text{ref}})}$ is termed the "reference unbalanced shaft speed". In the case of SFU, $\Omega_{(j_{\text{ref}})}$ is the speed of the (only) unbalanced shaft and $Q$ is commonly taken as 1. In the case of MFU, $\Omega_{(j_{\text{ref}})}$ is the speed of the slowest unbalanced shaft and the value of $Q$ will be chosen according to the ratio of the speeds of the unbalanced shafts (Section 3.2.2).

Let $x_{\mathrm{J}_i}$, $y_{\mathrm{J}_i}$ and $x_{\mathrm{B}_i}$, $y_{\mathrm{B}_i}$ be the instantaneous Cartesian displacements of the journal and housing centres $\mathrm{J}_i$, $\mathrm{B}_i$ at SFD no. $i$, both measured from the static equilibrium position of $\mathrm{B}_i$ under no rotor loading. Hence, if $\mathbf{x_J} = [x_{\mathrm{J}_1} \;\; y_{\mathrm{J}_1} \cdots x_{\mathrm{J}_N} \;\; y_{\mathrm{J}_N}]^{\mathrm{T}}$, $\mathbf{x_B} = [x_{\mathrm{B}_1} \;\; y_{\mathrm{B}_1} \cdots x_{\mathrm{B}_N} \;\; y_{\mathrm{B}_N}]^{\mathrm{T}}$, then:

$$\mathbf{x_J} = \bar{\mathbf{x}}_{\mathbf{J}} + \sum_{k=1}^{K} \{x^{(k)}_{\mathbf{J}\,\cos} \cos k\varpi t + x^{(k)}_{\mathbf{J}\,\sin} \sin k\varpi t\}, \tag{2a}$$

$$\mathbf{x_B} = \bar{\mathbf{x}}_{\mathbf{B}} + \sum_{k=1}^{K} \{x^{(k)}_{\mathbf{B}\,\cos} \cos k\varpi t + x^{(k)}_{\mathbf{B}\,\sin} \sin k\varpi t\}. \tag{2b}$$

Let $\boldsymbol{\rho}_i = [Q_{x_i} \;\; Q_{y_i}]^{\mathrm{T}}$ define the Cartesian forces on the journal $\mathrm{J}_i$ of SFD no. $i$, $i = 1 \ldots N$. The forces on the corresponding bearing housing $\mathrm{B}_i$ are hence given by $-\boldsymbol{\rho}_i$. Now $\boldsymbol{\rho}_i = \boldsymbol{\rho}_i(\mathbf{v}_i, \dot{\mathbf{v}}_i)$ where $\mathbf{v}_i = [x_{\mathrm{J}_i} - x_{\mathrm{B}_i} \;\; y_{\mathrm{J}_i} - y_{\mathrm{B}_i}]^{\mathrm{T}}$ and $\boldsymbol{\rho}_i = \boldsymbol{\rho}_i(\mathbf{v}_i, \dot{\mathbf{v}}_i)$ is calculated from the physical model of the SFD [1,6]. Hence,

$$\mathbf{v}_i = \bar{\mathbf{v}}_i + \sum_{k=1}^{K} \{\mathbf{v}^{(k)}_{i\,\cos} \cos k\varpi t + \mathbf{v}^{(k)}_{i\,\sin} \sin k\varpi t\}, \tag{3}$$

$$\boldsymbol{\rho}_i = \bar{\boldsymbol{\rho}}_i + \sum_{k=1}^{K} \{\boldsymbol{\rho}^{(k)}_{i\,\cos} \cos k\varpi t + \boldsymbol{\rho}^{(k)}_{i\,\sin} \sin k\varpi t\}, \tag{4}$$

where

$$\bar{\boldsymbol{\rho}}_i(\bar{\mathbf{v}}_i, \mathbf{v}_{i\,\cos}^{(1)}, \mathbf{v}_{i\,\sin}^{(1)}, \ldots, \mathbf{v}_{i\,\cos}^{(K)}, \mathbf{v}_{i\,\sin}^{(K)}) = (\varpi/(2\pi)) \int_0^{2\pi/\varpi} \boldsymbol{\rho}_i(\mathbf{v}_i, \dot{\mathbf{v}}_i)\, \mathrm{d}t, \tag{5a}$$

$$\boldsymbol{\rho}_{i\,\cos}^{(k)}(\bar{\mathbf{v}}_i, \mathbf{v}_{i\,\cos}^{(1)}, \mathbf{v}_{i\,\sin}^{(1)}, \ldots, \mathbf{v}_{i\,\cos}^{(K)}, \mathbf{v}_{i\,\sin}^{(K)}) = (\varpi/\pi) \int_0^{2\pi/\varpi} \boldsymbol{\rho}_i(\mathbf{v}_i, \dot{\mathbf{v}}_i) \cos k\varpi t\, \mathrm{d}t, \tag{5b}$$

$$\boldsymbol{\rho}_{i\,\sin}^{(k)}(\bar{\mathbf{v}}_i, \mathbf{v}_{i\,\cos}^{(1)}, \mathbf{v}_{i\,\sin}^{(1)}, \ldots, \mathbf{v}_{i\,\cos}^{(K)}, \mathbf{v}_{i\,\sin}^{(K)}) = (\varpi/\pi) \int_0^{2\pi/\varpi} \boldsymbol{\rho}_i(\mathbf{v}_i, \dot{\mathbf{v}}_i) \sin k\varpi t\, \mathrm{d}t. \tag{5c}$$

Hence, if

$$\mathbf{v} = \mathbf{x}_\mathbf{J} - \mathbf{x}_\mathbf{B} = \begin{bmatrix} \mathbf{v}_1 \\ \vdots \\ \mathbf{v}_N \end{bmatrix}, \tag{6}$$

$$\bar{\mathbf{v}} = \begin{bmatrix} \bar{\mathbf{v}}_1 \\ \vdots \\ \bar{\mathbf{v}}_N \end{bmatrix}, \tag{7a}$$

$$\mathbf{v}_{\cos}^{(k)} = \begin{bmatrix} \mathbf{v}_{1\,\cos}^{(k)} \\ \vdots \\ \mathbf{v}_{N\,\cos}^{(k)} \end{bmatrix}, \tag{7b}$$

$$\mathbf{v}_{\sin}^{(k)} = \begin{bmatrix} \mathbf{v}_{1\,\sin}^{(k)} \\ \vdots \\ \mathbf{v}_{N\,\sin}^{(k)} \end{bmatrix} \tag{7c}$$

then:

$$\bar{\boldsymbol{\rho}} = \begin{bmatrix} \bar{\boldsymbol{\rho}}_1 \\ \vdots \\ \bar{\boldsymbol{\rho}}_N \end{bmatrix} = \bar{\boldsymbol{\rho}}(\bar{\mathbf{v}}, \mathbf{v}_{\cos}^{(1)}, \mathbf{v}_{\sin}^{(1)}, \ldots, \mathbf{v}_{\cos}^{(K)}, \mathbf{v}_{\sin}^{(K)}), \tag{8a}$$

$$\boldsymbol{\rho}_{\cos}^{(k)} = \begin{bmatrix} \boldsymbol{\rho}_{1\,\cos}^{(k)} \\ \vdots \\ \boldsymbol{\rho}_{N\,\cos}^{(k)} \end{bmatrix} = \boldsymbol{\rho}_{\cos}^{(k)}(\bar{\mathbf{v}}, \mathbf{v}_{\cos}^{(1)}, v_{\sin}^{(1)}, \ldots, \mathbf{v}_{\cos}^{(1)}, \mathbf{v}_{\sin}^{(1)}), \tag{8b}$$

$$\boldsymbol{\rho}_{\sin}^{(k)} = \begin{bmatrix} \boldsymbol{\rho}_{1\,\sin}^{(k)} \\ \vdots \\ \boldsymbol{\rho}_{N\,\sin}^{(k)} \end{bmatrix} = \boldsymbol{\rho}_{\sin}^{(k)}(\bar{\mathbf{v}}, \mathbf{v}_{\cos}^{(1)}, \mathbf{v}_{\sin}^{(1)}, \ldots, \mathbf{v}_{\cos}^{(K)}, \mathbf{v}_{\sin}^{(K)}). \tag{8c}$$

For the $j$th rotor the unbalances $U_{(j)1},\ldots U_{(j)S_j}$ are concentrated at $S_j$ points. The vector of unbalance excitations on rotor no. $j$ can be written as

$$\mathbf{u}_{(j)} = \mathbf{u}_{(j)\ \cos}\ \cos\ \Omega_{(j)}t + \mathbf{u}_{(j)\ \sin}\ \sin\ \Omega_{(j)}t, \tag{9}$$

where

$$\mathbf{u}_{(j)\cos} = \Omega_{(j)}^2 \begin{bmatrix} U_{(j)1}\ \sin(\phi_{(j)} + \gamma_{(j)1}) \\ -U_{(j)1}\ \cos(\phi_{(j)} + \gamma_{(j)1}) \\ \vdots \\ U_{(j)S_j}\ \sin(\phi_{(j)} + \gamma_{(j)S_j}) \\ -U_{(j)S_j}\ \cos(\phi_{(j)} + \gamma_{(j)S_j}) \end{bmatrix}, \tag{10a}$$

$$\mathbf{u}_{(j)\ \sin} = \Omega_{(j)}^2 \begin{bmatrix} U_{(j)1}\ \cos(\phi_{(j)} + \gamma_{(j)1}) \\ U_{(j)1}\ \sin(\phi_{(j)} + \gamma_{(j)1}) \\ \vdots \\ U_{(j)S_j}\ \cos(\phi_{(j)} + \gamma_{(j)S_j}) \\ U_{(j)S_j}\ \sin(\phi_{(j)} + \gamma_{(j)S_j}) \end{bmatrix}. \tag{10b}$$

$\gamma_{(j)s}$, $s = 1\ldots S_j$, is the angular position of the unbalance at location no. $s$ of rotor no. $j$ relative to the angular position of unbalance no. 1 on the *same* rotor ($\gamma_{(j)1} = 0$ for all $j$). $\phi_{(j)}$ is the angular position of unbalance no. 1 on rotor no. $j$ relative to the angular position of unbalance no. 1 on rotor no. 1 *at the instant* $t = 0$ ($\phi_{(1)} = 0$). It is to be noted that, for a given unbalance distribution on the engine, the values of $\gamma_{(j,s)}$ are fixed but the values of $\phi_{(j)}$ ($j = 2, 3\ldots$) are arbitrary since the angular positions of the rotors relative to each other at the reference time $t = 0$ are arbitrary.

For the $j$th rotor the gyroscopic effects are concentrated at $G_j$ points. Let $\mathbf{g}$ be the vector containing the gyroscopic moments on all the rotors. Hence:

$$\mathbf{g} = \mathbf{P}\dot{\boldsymbol{\theta}}, \tag{11}$$

where $\mathbf{g}$, $\mathbf{P}$, and the vector $\boldsymbol{\theta}$ of flexural rotations at the gyroscopic locations are defined in the Nomenclature. Due to the periodicity of the vibration and as a result of Eq. (11), one can write:

$$\boldsymbol{\theta} = \bar{\boldsymbol{\theta}} + \sum_{k=1}^{K} \{\boldsymbol{\theta}_{\cos}^{(k)}\ \cos\ k\varpi t + \boldsymbol{\theta}_{\sin}^{(k)}\ \sin\ k\varpi t\}, \tag{12}$$

$$\mathbf{g} = \sum_{k=1}^{K} \{\mathbf{g}_{\cos}^{(k)}\ \cos\ k\varpi t + \mathbf{g}_{\sin}^{(k)}\ \sin\ k\varpi t\}, \tag{13}$$

where

$$\mathbf{g}_{\cos}^{(k)} = k\varpi \mathbf{P}\boldsymbol{\theta}_{\sin}^{(k)}, \tag{14a}$$

$$\mathbf{g}_{\sin}^{(k)} = -k\varpi \mathbf{P}\boldsymbol{\theta}_{\cos}^{(k)}. \tag{14b}$$

### 2.2. Derivation of the block of dynamic equations

For each harmonic $k\varpi$, $k = 1 \ldots K$, of the response at the SFDs (Eqs. (2a) and (2b)) one can write the following force–displacement relationships:

$$\begin{bmatrix} \mathbf{x}_{\mathbf{J}\,\cos}^{(k)} \\ \mathbf{x}_{\mathbf{J}\,\sin}^{(k)} \end{bmatrix} = \begin{bmatrix} \mathbf{C}_{\mathbf{JJ}}(k\varpi) & \mathbf{0} \\ \mathbf{0} & \mathbf{C}_{\mathbf{JJ}}(k\varpi) \end{bmatrix} \begin{bmatrix} \boldsymbol{\rho}_{\cos}^{(k)} \\ \boldsymbol{\rho}_{\sin}^{(k)} \end{bmatrix} + \begin{bmatrix} \mathbf{C}_{\mathbf{JB}}(k\varpi) & \mathbf{0} \\ \mathbf{0} & \mathbf{C}_{\mathbf{JB}}(k\varpi) \end{bmatrix} \begin{bmatrix} -\boldsymbol{\rho}_{\cos}^{(K)} \\ -\boldsymbol{\rho}_{\sin}^{(K)} \end{bmatrix} + \begin{bmatrix} \mathbf{C}_{\mathbf{Jg}}(k\varpi) & \mathbf{0} \\ \mathbf{0} & \mathbf{C}_{\mathbf{Jg}}(k\varpi) \end{bmatrix} \begin{bmatrix} \mathbf{g}_{\cos}^{(k)} \\ \mathbf{g}_{\sin}^{(k)} \end{bmatrix} + \sum_{j=1}^{J} \delta_{k\varpi,\Omega_{(j)}} \begin{bmatrix} \mathbf{C}_{\mathbf{Ju}_{(j)}}(k\varpi) & \mathbf{0} \\ \mathbf{0} & \mathbf{C}_{\mathbf{Ju}_{(j)}}(k\varpi) \end{bmatrix} \begin{bmatrix} \mathbf{u}_{(j)\cos} \\ \mathbf{u}_{(j)\sin} \end{bmatrix}, \quad k = 1 \ldots K, \tag{15a}$$

$$\begin{bmatrix} \mathbf{x}_{\mathbf{B}\,\cos}^{(k)} \\ \mathbf{x}_{\mathbf{B}\,\sin}^{(k)} \end{bmatrix} = \begin{bmatrix} \mathbf{C}_{\mathbf{BJ}}(k\varpi) & \mathbf{0} \\ \mathbf{0} & \mathbf{C}_{\mathbf{BJ}}(k\varpi) \end{bmatrix} \begin{bmatrix} \boldsymbol{\rho}_{\cos}^{(k)} \\ \boldsymbol{\rho}_{\sin}^{(k)} \end{bmatrix} + \begin{bmatrix} \mathbf{C}_{\mathbf{BB}}(k\varpi) & \mathbf{0} \\ \mathbf{0} & \mathbf{C}_{\mathbf{BB}}(k\varpi) \end{bmatrix} \begin{bmatrix} -\boldsymbol{\rho}_{\cos}^{(k)} \\ -\boldsymbol{\rho}_{\sin}^{(k)} \end{bmatrix} + \begin{bmatrix} \mathbf{C}_{\mathbf{Bg}}(k\varpi) & \mathbf{0} \\ \mathbf{0} & \mathbf{C}_{\mathbf{Bg}}(k\varpi) \end{bmatrix} \begin{bmatrix} \mathbf{g}_{\cos}^{(k)} \\ \mathbf{g}_{\sin}^{(k)} \end{bmatrix} + \sum_{j=1}^{J} \delta_{k\varpi,\Omega_{(j)}} \begin{bmatrix} \mathbf{C}_{\mathbf{Bu}_{(j)}}(k\varpi) & \mathbf{0} \\ \mathbf{0} & \mathbf{C}_{\mathbf{Bu}_{(j)}}(k\varpi) \end{bmatrix} \begin{bmatrix} \mathbf{u}_{(j)\cos} \\ \mathbf{u}_{(j)\sin} \end{bmatrix}, \quad k = 1 \ldots K. \tag{15b}$$

In above equations, the receptance (or "compliance") matrices are defined from modal theory [9] as

$$\mathbf{C}_{\mathbf{JJ}}(\omega) = \sum_{r=1}^{R} \frac{\boldsymbol{\psi}_{\mathbf{J}}^{(r)} \boldsymbol{\psi}_{\mathbf{J}}^{(r)\mathrm{T}}}{\omega_r^2 - \omega^2}, \tag{16a}$$

$$\mathbf{C}_{\mathbf{JB}}(\omega) = \mathbf{C}_{\mathbf{BJ}}(\omega) = \sum_{r=1}^{R} \frac{\boldsymbol{\psi}_{\mathbf{J}}^{(r)} \boldsymbol{\psi}_{\mathbf{B}}^{(r)\mathrm{T}}}{\omega_r^2 - \omega^2}, \tag{16b}$$

$$\mathbf{C}_{\mathbf{Jg}}(\omega) = \sum_{r=1}^{R} \frac{\boldsymbol{\psi}_{\mathbf{J}}^{(r)} \boldsymbol{\psi}_{\mathbf{g}}^{(r)\mathrm{T}}}{\omega_r^2 - \omega^2}, \tag{16c}$$

$$\mathbf{C}_{\mathbf{Ju}_{(j)}}(\omega) = \sum_{r=1}^{R} \frac{\boldsymbol{\psi}_{\mathbf{J}}^{(r)} \boldsymbol{\psi}_{\mathbf{u}_{(j)}}^{(r)\mathrm{T}}}{\omega_r^2 - \omega^2}, \tag{16d}$$

$$\mathbf{C}_{\mathbf{BB}}(\omega) = \sum_{r=1}^{R} \frac{\boldsymbol{\psi}_{\mathbf{B}}^{(r)} \boldsymbol{\psi}_{\mathbf{B}}^{(r)\mathrm{T}}}{\omega_r^2 - \omega^2}, \tag{16e}$$

$$\mathbf{C}_{\mathbf{Bg}}(\omega) = \sum_{r=1}^{R} \frac{\boldsymbol{\psi}_{\mathbf{B}}^{(r)} \boldsymbol{\psi}_{\mathbf{g}}^{(r)\mathrm{T}}}{\omega_r^2 - \omega^2}, \tag{16f}$$

$$\mathbf{C}_{\mathbf{Bu}_{(j)}}(\omega) = \sum_{r=1}^{R} \frac{\boldsymbol{\psi}_{\mathbf{B}}^{(r)} \boldsymbol{\psi}_{\mathbf{u}_{(j)}}^{(r)\mathrm{T}}}{\omega_r^2 - \omega^2}. \tag{16g}$$

In the above expressions, $\omega_r$ ($r = 1 \ldots R$) are the undamped natural frequencies of the linear part. $\boldsymbol{\psi}_{\mathbf{J}}^{(r)}$, $\boldsymbol{\psi}_{\mathbf{B}}^{(r)}$ are the mass-normalised eigenvectors defining the $x$, $y$ displacements of the squeeze-film terminals $\mathrm{J}_i$, $\mathrm{B}_i$ in mode no. $r$. Similarly, $\boldsymbol{\psi}_{\mathbf{u}_{(j)}}^{(r)}$, $\boldsymbol{\psi}_{\mathbf{g}}^{(r)}$ are mass-normalised eigenvectors taken at the degrees of freedom corresponding to the directions and locations of the elements of $\mathbf{u}_{(j)}$ and $\mathbf{g}$, respectively. Defining

$$\boldsymbol{\psi}_{\mathbf{v}}^{(r)} = \boldsymbol{\psi}_{\mathbf{J}}^{(r)} - \psi_{\mathbf{B}}^{(r)}. \tag{17}$$

Subtracting Eq. (15b) from Eq. (15a), and using relations (16a)–(16g) one obtains:

$$\begin{bmatrix}\mathbf{v}_{\cos}^{(k)}\\ \mathbf{v}_{\sin}^{(k)}\end{bmatrix}=\begin{bmatrix}\mathbf{C}_{\mathbf{vv}}(k\varpi) & \mathbf{0}\\ \mathbf{0} & \mathbf{C}_{\mathbf{vv}}(k\varpi)\end{bmatrix}\begin{bmatrix}\boldsymbol{\rho}_{\cos}^{(k)}\\ \boldsymbol{\rho}_{\sin}^{(k)}\end{bmatrix}+\begin{bmatrix}\mathbf{C}_{\mathbf{vg}}(k\varpi) & \mathbf{0}\\ \mathbf{0} & \mathbf{C}_{\mathbf{vg}}(k\varpi)\end{bmatrix}\begin{bmatrix}\mathbf{g}_{\cos}^{(k)}\\ \mathbf{g}_{\sin}^{(k)}\end{bmatrix}+\sum_{j=1}^{J}\delta_{k\varpi,\Omega_{(j)}}\begin{bmatrix}\mathbf{C}_{\mathbf{vu}_{(j)}}(k\varpi) & \mathbf{0}\\ \mathbf{0} & \mathbf{C}_{\mathbf{vu}_{(j)}}(k\varpi)\end{bmatrix}\begin{bmatrix}\mathbf{u}_{(j)\cos}\\ \mathbf{u}_{(j)\sin}\end{bmatrix},\quad k=1\ldots K, \tag{18}$$

where

$$\mathbf{C}_{\mathbf{vv}}(\omega)=\sum_{r=1}^{R}\frac{\boldsymbol{\psi}_{\mathbf{v}}^{(r)}\boldsymbol{\psi}_{\mathbf{v}}^{(r)\mathrm{T}}}{\omega_r^2-\omega^2}, \tag{19a}$$

$$\mathbf{C}_{\mathbf{vg}}(\omega)=\sum_{r=1}^{R}\frac{\boldsymbol{\psi}_{\mathbf{v}}^{(r)}\boldsymbol{\psi}_{\mathbf{g}}^{(r)\mathrm{T}}}{\omega_r^2-\omega^2}, \tag{19b}$$

$$\mathbf{C}_{\mathbf{vu}_{(j)}}(\omega)=\sum_{r=1}^{R}\frac{\boldsymbol{\psi}_{\mathbf{v}}^{(r)}\boldsymbol{\psi}_{\mathbf{u}_{(j)}}^{(r)\mathrm{T}}}{\omega_r^2-\omega^2}. \tag{19c}$$

The above matrices can be regarded compliance matrices relating the *relative* responses at the SFD terminals to the various excitations.

The gyroscopic terms $\mathbf{g}_{\cos}^{(k)}$, $\mathbf{g}_{\sin}^{(k)}$ can be eliminated from the right-hand side of Eq. (18) as follows. By analogy with Eq. (18), one can write a force–displacement relationship for each harmonic $k\varpi$ of the flexural angular displacement $\boldsymbol{\theta}$ at the gyroscopic locations:

$$\begin{bmatrix}\boldsymbol{\theta}_{\cos}^{(k)}\\ \boldsymbol{\theta}_{\sin}^{(k)}\end{bmatrix}=\begin{bmatrix}\mathbf{C}_{\boldsymbol{\theta}\mathbf{v}}(k\varpi) & \mathbf{0}\\ \mathbf{0} & \mathbf{C}_{\boldsymbol{\theta}\mathbf{v}}(k\varpi)\end{bmatrix}\begin{bmatrix}\boldsymbol{\rho}_{\cos}^{(k)}\\ \boldsymbol{\rho}_{\sin}^{(k)}\end{bmatrix}+\begin{bmatrix}\mathbf{C}_{\boldsymbol{\theta}\mathbf{g}}(k\varpi) & \mathbf{0}\\ \mathbf{0} & \mathbf{C}_{\boldsymbol{\theta}\mathbf{g}}(k\varpi)\end{bmatrix}\begin{bmatrix}\mathbf{g}_{\cos}^{(k)}\\ \mathbf{g}_{\sin}^{(k)}\end{bmatrix}+\sum_{j=1}^{J}\delta_{k\varpi,\Omega_{(j)}}\begin{bmatrix}\mathbf{C}_{\boldsymbol{\theta}\mathbf{u}_{(j)}}(k\varpi) & \mathbf{0}\\ \mathbf{0} & \mathbf{C}_{\boldsymbol{\theta}\mathbf{u}_{(j)}}(k\varpi)\end{bmatrix}\begin{bmatrix}\mathbf{u}_{(j)\cos}\\ \mathbf{u}_{(j)\sin}\end{bmatrix}, \tag{20}$$

where

$$\mathbf{C}_{\boldsymbol{\theta}\mathbf{v}}(k\varpi)=\sum_{r=1}^{R}\frac{\boldsymbol{\psi}_{\boldsymbol{\theta}}^{(r)}\boldsymbol{\psi}_{\mathbf{v}}^{(r)\mathrm{T}}}{\omega_r^2-\omega^2}, \tag{21a}$$

$$\mathbf{C}_{\boldsymbol{\theta}\mathbf{g}}(k\varpi)=\sum_{r=1}^{R}\frac{\boldsymbol{\psi}_{\boldsymbol{\theta}}^{(r)}\boldsymbol{\psi}_{\mathbf{g}}^{(r)\mathrm{T}}}{\omega_r^2-\omega^2}, \tag{21b}$$

$$\mathbf{C}_{\boldsymbol{\theta}\mathbf{u}_{(j)}}(k\varpi)=\sum_{r=1}^{R}\frac{\boldsymbol{\psi}_{\boldsymbol{\theta}}^{(r)}\boldsymbol{\psi}_{\mathbf{u}_{(j)}}^{(r)\mathrm{T}}}{\omega_r^2-\omega^2}. \tag{21c}$$

$\ldots\boldsymbol{\psi}_{\boldsymbol{\theta}}^{(r)}$ being mass-normalised eigenvectors taken at the degrees of freedom corresponding to the elements in $\boldsymbol{\theta}$. Substituting for $\mathbf{g}_{\cos}^{(k)}$, $\mathbf{g}_{\sin}^{(k)}$ from Eqs. (14a) and (14b) into Eq. (20) and solving the resulting equations for $\boldsymbol{\theta}_{\cos}^{(k)}$, $\boldsymbol{\theta}_{\sin}^{(k)}$ one obtains

$$\begin{bmatrix}\boldsymbol{\theta}_{\sin}^{(k)}\\ \boldsymbol{\theta}_{\cos}^{(k)}\end{bmatrix}=\begin{bmatrix}-\mathbf{D}(k\varpi)\mathbf{B}(k\varpi)\mathbf{C}_{\boldsymbol{\theta}\mathbf{v}}(k\varpi) & \mathbf{D}(k\varpi)\mathbf{C}_{\boldsymbol{\theta}\mathbf{v}}(k\varpi)\\ \mathbf{D}(k\varpi)\mathbf{C}_{\boldsymbol{\theta}\mathbf{v}}(k\varpi) & \mathbf{D}(k\varpi)\mathbf{B}(k\varpi)\mathbf{C}_{\boldsymbol{\theta}\mathbf{v}}(k\varpi)\end{bmatrix}\begin{bmatrix}\boldsymbol{\rho}_{\cos}^{(k)}\\ \boldsymbol{\rho}_{\sin}^{(k)}\end{bmatrix}+\sum_{j=1}^{J}\delta_{k\varpi,\Omega_{(j)}}\begin{bmatrix}-\mathbf{D}(k\varpi)\mathbf{B}(k\varpi)\mathbf{C}_{\boldsymbol{\theta}\mathbf{u}_{(j)}}(k\varpi) & \mathbf{D}(k\varpi)\mathbf{C}_{\boldsymbol{\theta}\mathbf{u}_{(j)}}(k\varpi)\\ \mathbf{D}k\varpi\mathbf{C}_{\boldsymbol{\theta}\mathbf{u}_{(j)}}(k\varpi) & \mathbf{D}(k\varpi)\mathbf{B}(k\varpi)\mathbf{C}_{\boldsymbol{\theta}\mathbf{u}_{(j)}}(k\varpi)\end{bmatrix}\begin{bmatrix}\mathbf{u}_{(j)\cos}\\ \mathbf{u}_{(j)\sin}\end{bmatrix}, \tag{22}$$

where

$$\mathbf{D}(k\varpi) = (\mathbf{I} + \mathbf{B}(k\varpi)^2)^{-1}, \tag{23a}$$

$$\mathbf{B}(k\varpi) = k\varpi \mathbf{C}_{\boldsymbol{\theta}\mathbf{g}}(k\varpi)\mathbf{P}. \tag{23b}$$

Hence, from Eqs. (14a) and (14b) and Eq. (22), one can eliminate $\mathbf{g}_{\cos}^{(k)}$, $\mathbf{g}_{\sin}^{(k)}$ from Eq. (18):

$$\begin{bmatrix} \mathbf{v}_{\cos}^{(k)} \\ \mathbf{v}_{\sin}^{(k)} \end{bmatrix} = \begin{bmatrix} \mathbf{C}_{\mathbf{vv}}(k\varpi) - \mathbf{E}(k\varpi) & \mathbf{F}(k\varpi) \\ -\mathbf{F}(k\varpi) & \mathbf{C}_{\mathbf{vv}}(k\varpi) - \mathbf{E}(k\varpi) \end{bmatrix} \begin{bmatrix} \boldsymbol{\rho}_{\cos}^{(k)} \\ \boldsymbol{\rho}_{\sin}^{(k)} \end{bmatrix} + \sum_{j=1}^{J} \delta_{k\varpi,\Omega_{(j)}} \begin{bmatrix} \mathbf{C}_{\mathbf{vu}_{(j)}}(k\varpi) - \mathbf{L}_{(j)}(k\varpi) & \mathbf{Q}_{(j)}(k\varpi) \\ -\mathbf{Q}_{(j)}(k\varpi) & \mathbf{C}_{\mathbf{vu}_{(j)}}(k\varpi) - \mathbf{L}_{(j)}(k\varpi) \end{bmatrix} \begin{bmatrix} \mathbf{u}_{(j)\cos} \\ \mathbf{u}_{(j)\sin} \end{bmatrix}, \quad k = 1 \ldots K, \tag{24}$$

where

$$\mathbf{E}(k\varpi) = k\varpi \mathbf{C}_{\mathbf{vg}}(k\varpi)\mathbf{P}\mathbf{D}(k\varpi)\mathbf{B}(k\varpi)\mathbf{C}_{\boldsymbol{\theta}\mathbf{v}}(k\varpi), \tag{25a}$$

$$\mathbf{F}(k\varpi) = k\varpi \mathbf{C}_{\mathbf{vg}}(k\varpi)\mathbf{P}\mathbf{D}(k\varpi)\mathbf{C}_{\boldsymbol{\theta}\mathbf{v}}(k\varpi), \tag{25b}$$

$$\mathbf{L}_{(j)}(k\varpi) = k\varpi \mathbf{C}_{\mathbf{vg}}(k\varpi)\mathbf{P}\mathbf{D}(k\varpi)\mathbf{B}(k\varpi)\mathbf{C}_{\boldsymbol{\theta}\mathbf{u}_{(j)}}(k\varpi), \tag{25c}$$

$$\mathbf{Q}_{(j)}(k\varpi) = k\varpi \mathbf{C}_{\mathbf{vg}}(k\varpi)\mathbf{P}\mathbf{D}(k\varpi)\mathbf{C}_{\boldsymbol{\theta}\mathbf{u}_{(j)}}(k\varpi). \tag{25d}$$

Eq. (24) constitute the dynamic block of the RHBM equations. By consideration of the relationships in Eqs. (8a)–(8c), it is clear that Eqs. (24) constitute a set of $2N \times 2K$ equations in $2N \times (2K + 1)$ unknowns (which are the Fourier coefficients of the relative displacements at the SFDs, Eqs. (7a)–(7c)). A block of "pseudo-static" equations (defining force–response relations at zero-frequency) will complete the equation set.

### 2.3. Derivation of the block of pseudo-static equations

As can be seen from Eq. (19a), the presence of rigid body modes (for which $\omega_r = 0$) in the linear part, would result in the receptance matrix $\mathbf{C}_{\mathbf{vv}}(0) \to \pm\infty$. Note that the rigid body modes define rigid body motion of one or more rotors in the *xz* or *yz* planes (the superfluous modes defining rigid body spin of each rotor about its axis are removed). As discussed in the Introduction, $\bar{\boldsymbol{\rho}}$ and the static loading $\mathbf{w}$ are in equilibrium. This principle can be applied in a systematic fashion by writing zero-frequency force–acceleration response equations at *selected* journals $\mathrm{J}_i$ as follows:

$$\mathbf{0} = \mathbf{A}_{\mathbf{J}_{\mathrm{sel}}\mathbf{v}}(0)\bar{\boldsymbol{\rho}} + \mathbf{A}_{\mathbf{J}_{\mathrm{sel}}\mathbf{w}}(0)\mathbf{w}, \tag{26}$$

where the accelerance matrices are defined as

$$\mathbf{A}_{\mathbf{J}_{\mathrm{sel}}\mathbf{v}}(\omega) = \sum_{r=1}^{R} -\omega^2 \frac{\boldsymbol{\psi}_{\mathbf{J}_{\mathrm{sel}}}^{(r)} \boldsymbol{\psi}_{\mathbf{v}}^{(r)\mathrm{T}}}{\omega_r^2 - \omega^2}, \tag{27a}$$

$$\mathbf{A}_{\mathbf{J}_{\mathrm{sel}}\mathbf{w}}(\omega) = \sum_{r=1}^{R} -\omega^2 \frac{\boldsymbol{\psi}_{\mathbf{J}_{\mathrm{sel}}}^{(r)} \boldsymbol{\psi}_{\mathbf{w}}^{(r)\mathrm{T}}}{\omega_r^2 - \omega^2}. \tag{27b}$$

$\boldsymbol{\psi}_{\mathbf{J}_{\mathrm{sel}}}^{(r)}$ are the mass-normalised eigenvectors defining the *x*, *y* displacements at the selected journals $\mathrm{J}_i$. If the linear part has a total of *P* rigid body modes i.e. $\omega_1 \ldots \omega_P = 0$, then:

$$\mathbf{A}_{\mathbf{J}_{\mathrm{sel}}\mathbf{v}}(0) = \sum_{r=1}^{P} \boldsymbol{\psi}_{\mathbf{J}_{\mathrm{sel}}}^{(r)} \boldsymbol{\psi}_{\mathbf{v}}^{(r)\mathrm{T}}, \tag{28a}$$

$$\mathbf{A}_{\mathbf{J}_{\mathrm{sel}}\mathbf{w}}(0) = \sum_{r=1}^{P} \boldsymbol{\psi}_{\mathbf{J}_{\mathrm{sel}}}^{(r)} \boldsymbol{\psi}_{\mathbf{w}}^{(r)\mathrm{T}}. \tag{28b}$$

In the case of the engine shown in Fig. 1, $P = 4$, since each rotor has two rigid body modes: one per plane $xz$, $yz$, defining pivoting motion about $J_1$ or $J_3$. Eqs. (26) effectively define moment equilibrium in each plane about each pivot. In general, the method of Eq. (26) yields a maximum of $P$ independent equations. Hence, it is for this reason that Eq. (26) is only applied at *selected* journals $J_i$. The selection is arbitrary provided that none of the chosen journals is a node (pivot) in the corresponding rotor's rigid body modes since it would then introduce trivial "$0 = 0$" equations in the corresponding rows of Eq. (26).

Since the total number of unknown Fourier coefficients of the relative displacement at the SFDs (Eqs. (7a)–(7c)) is $2N \times (2K + 1)$, then from the above it is apparent that if $P < 2N$ additional zero-frequency equations need to be found to supplement Eq. (26).

Let $\mathbf{q}$ be the vector of instantaneous modal coordinates, which represent the vibration of the structure in modal space. Due to the periodicity of the vibration:

$$\mathbf{q} = \bar{\mathbf{q}} + \sum_{k=1}^{K} \{\mathbf{q}_{\cos}^{(k)} \cos k\varpi t + \mathbf{q}_{\sin}^{(k)} \sin k\varpi t\}. \tag{29}$$

Let the mean component vector $\bar{\mathbf{q}}$ be partitioned thus:

$$\bar{\mathbf{q}} = [\bar{\tilde{\mathbf{q}}}^{\mathrm{T}} \;\; \bar{\check{\mathbf{q}}}^{\mathrm{T}}]^{\mathrm{T}}, \tag{30}$$

where $\bar{\tilde{\mathbf{q}}}$ is the $P \times 1$ vector of mean modal coordinates associated with the rigid body modes. Hence, the additional block of zero-frequency equations is given as follows, by splitting the response into rigid and flexible modal contributions:

$$\bar{\mathbf{v}} - \mathbf{v}_{\mathbf{s}} = \check{\mathbf{H}}_{\mathbf{v}} \bar{\tilde{\mathbf{q}}} + \tilde{\mathbf{C}}_{\mathbf{vv}}(0)\bar{\boldsymbol{\rho}} + \tilde{\mathbf{C}}_{\mathbf{vw}}(0)\mathbf{w}. \tag{31}$$

In Eq. (31), $\mathbf{v}_{\mathbf{s}}$ is a vector defining the static offsets of the SFD journals relative to their housings, in the $x$, $y$ directions, under no rotor loading. $\check{\mathbf{H}}_{\mathbf{v}}$ is the rigid body modal matrix defined by

$$\check{\mathbf{H}}_{\mathbf{v}} = [\boldsymbol{\psi}_{\mathbf{v}}^{(1)} \;\; \cdots \;\; \boldsymbol{\psi}_{\mathbf{v}}^{(P)}]. \tag{32}$$

$\tilde{\mathbf{C}}_{\mathbf{vv}}(0), \tilde{\mathbf{C}}_{\mathbf{vw}}(0)$ are zero-frequency "incomplete" compliance matrices with the rigid body mode contribution excluded i.e.:

$$\tilde{\mathbf{C}}_{\mathbf{vv}}(\omega) = \sum_{r=P+1}^{R} \frac{\boldsymbol{\psi}_{\mathbf{v}}^{(r)} \boldsymbol{\psi}_{\mathbf{v}}^{(r)\mathrm{T}}}{\omega_r^2 - \omega^2}, \tag{33a}$$

$$\tilde{\mathbf{C}}_{\mathbf{vw}}(\omega) = \sum_{r=P+1}^{R} \frac{\boldsymbol{\psi}_{\mathbf{v}}^{(r)} \boldsymbol{\psi}_{\mathbf{w}}^{(r)\mathrm{T}}}{\omega_r^2 - \omega^2}. \tag{33b}$$

The block of zero-frequency equations can thus be expressed as follows, for the most general case:

$$\begin{bmatrix} \mathbf{0} \\ \bar{\mathbf{v}} - \mathbf{v}_{\mathbf{s}} \end{bmatrix} = \begin{bmatrix} \mathbf{0}_{P \times P} \\ \check{\mathbf{H}}_{\mathbf{v}} \end{bmatrix} \bar{\tilde{\mathbf{q}}} + \begin{bmatrix} \mathbf{A}_{\mathbf{J}_{\mathrm{sel}}\mathbf{v}}(0) \\ \tilde{\mathbf{C}}_{\mathbf{vv}}(0) \end{bmatrix} \bar{\boldsymbol{\rho}} + \begin{bmatrix} \mathbf{A}_{\mathbf{J}_{\mathrm{sel}}\mathbf{w}}(0)\mathbf{w} \\ \tilde{\mathbf{C}}_{\mathbf{vw}}(0)\mathbf{w} \end{bmatrix}. \tag{34}$$

It is observed that an extra $P$ zero-frequency unknowns, contained in $\bar{\tilde{\mathbf{q}}}$, have been introduced into the system, in addition to the $2N$ zero-frequency unknowns in $\bar{\mathbf{v}}$. However, this is not a problem since there are $P + 2N$ equations in Eq. (34). The extra unknowns term $\bar{\tilde{\mathbf{q}}}$ in Eq. (34) either vanishes or is not required for the following two special cases:

(a) $P = 2N$ — *zero-frequency equations* "*fully implicit*": In this case Eq. (31) (i.e. the lower row set of Eq. (34), and consequently $\bar{\tilde{\mathbf{q}}}$) is not required. One example of this case would be if each rotor in Fig. 1 had only two bearings, all of which were unsupported SFDs.

(b) $P = 0$ — *zero-frequency equations* "*fully explicit*": In this case the upper row set of Eq. (34) and $\check{\mathbf{H}}_{\mathbf{v}}$ are null and only the lower row set is used. This would occur if each rotor in Fig. 1 had retainer springs at two or more SFDs.

The introduction of the extra unknowns term $\bar{\bar{\mathbf{q}}}$ allows the resolution of the first of the outstanding issues bulleted in the latter part of the Introduction i.e. the solution of systems involving at least one rotor that is statically indeterminate with the nonlinear elements in place and either does not have any linear support or has just one linear point support (as clearly evident for the LP rotor in Fig. 1).

### 2.4. Solution of the equations

Eqs. (24) and (34) together constitute the full set of $2N(2K+1)+n_{\text{extra}}$ nonlinear algebraic equations in an equal number of unknowns (where $n_{\text{extra}}=P$, except for the special cases (a) and (b) in previous section where $n_{\text{extra}}=0$). Collecting the unknowns into one vector

$$\mathbf{z}=[\bar{\bar{\mathbf{q}}}^{\mathrm{T}}\ \ \bar{\mathbf{v}}^{\mathrm{T}}\ \ \mathbf{v}_{\cos}^{(1)\mathrm{T}}\ \ \mathbf{v}_{\sin}^{(1)\mathrm{T}}\ \ldots\mathbf{v}_{\cos}^{(K)\mathrm{T}}\ \ \mathbf{v}_{\sin}^{(K)\mathrm{T}}]^{\mathrm{T}} \tag{35}$$

and moving all terms of Eqs. (24) and (34) to the left-hand side, the system of equations can be expressed as

$$\boldsymbol{\chi}(\mathbf{z},\Omega_{(j_{\text{ref}})},Q)=\mathbf{0}, \tag{36}$$

where $\boldsymbol{\chi}$ is a nonlinear vector function of $\mathbf{z}$, $\Omega_{(j_{\text{ref}})}$ and $Q$. This is due to the fact that, for given $\Omega_{(j_{\text{ref}})}$, $Q$ (Eq. (1)) and an assumed $\mathbf{z}$, all terms in Eqs. (24) and (34) are fully determined. In particular, the terms $\bar{\boldsymbol{\rho}}$, $\boldsymbol{\rho}_{\cos}^{(k)}$, $\boldsymbol{\rho}_{\sin}^{(k)}$ are calculated as indicated in the flow chart of Fig. 3.

Hence, for given $\Omega_{(j_{\text{ref}})}$ and $Q$ the Eq. (36) can be solved for $\mathbf{z}$ by iteration. Eq. (36) can be solved over a range of $\Omega_{(j_{\text{ref}})}$ for given $Q$ to yield a set of solutions defining a "speed response curve". In the case of MFU, a fixed $Q$ implies that the ratio of the speeds of the rotors is kept fixed as the speed $\Omega_{(j_{\text{ref}})}$ is varied. The continuation technique used to advance the solution procedure along the curve uses a predictor-corrector approach [6] where the initial approximation (or "predictor") $\mathbf{z}_0$ for the solution $\mathbf{z}$ at a point on the curve is obtained from the previous points. Eq. (36) is then solved by the damped Newton–Raphson method (the "corrector") [10]. The initial approximation for the first point on the curve is furnished by the Fourier coefficients of a time-marching solution.

At each point on the speed response, the Newton–Raphson method requires the calculation of the Jacobian matrix $\partial\boldsymbol{\chi}/\partial\mathbf{z}|_{\mathbf{z}=\mathbf{z}_0}$, which is then inverted. As $\mathbf{z}$ iterates towards its correct value the inverse of the Jacobian is efficiently updated using Broyden's Method [10]. In view of the large number of unknowns and the process of Fig. 3 (which is applied as many times as necessary during the iterative process), an efficient means of computing the Jacobian is imperative. From Eqs. (24) and (34) it is clear that the computational burden lies the evaluation of the matrices $\partial\bar{\boldsymbol{\rho}}/\partial\mathbf{z}$, $\partial\boldsymbol{\rho}_{\cos}^{(k)}/\partial\mathbf{z}$, $\partial\boldsymbol{\rho}_{\sin}^{(k)}/\partial\mathbf{z}$. Appendix A gives a method to assemble these matrices efficiently from the partial derivatives of the Fourier coefficients of the forces at each SFD no. $i$ with respect to the Fourier coefficients of its own relative displacements.

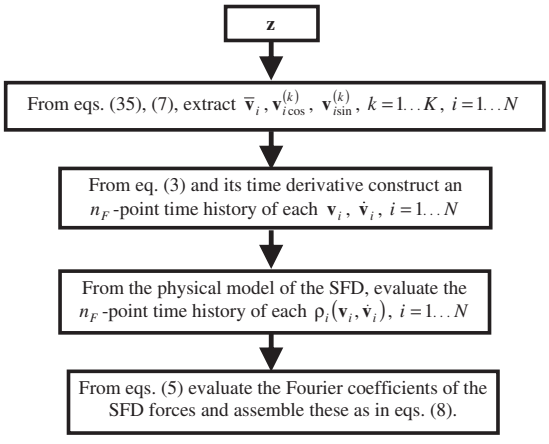


Fig. 3. Calculation of SFD force Fourier coefficients $\bar{\boldsymbol{\rho}}$, $\boldsymbol{\rho}_{\cos}^{(k)}$, $\boldsymbol{\rho}_{\sin}^{(k)}$ for assumed $\mathbf{z}$.

### 2.5. Recovery of the full set of degrees of freedom

Having solved for $\mathbf{z}$, the definitive values of the Fourier coefficients of the SFD forces and the gyroscopic moments can be determined (the latter found from Eqs. (14a), (14b) and (22)). These enable the computation of the Fourier coefficients of the vector of modal coordinates $\mathbf{q}$ (Eq. (29)). This in turn allows the computation of the time history of the response at a set of arbitrary degrees of freedom $\mathbf{x_P}$ since $\mathbf{x_P} = \mathbf{H_P q}$ where $\mathbf{H_P}$ is a matrix of mass-normalised eigenvectors evaluated at the degrees of freedom $\mathbf{x_P}$. The Fourier coefficients of $\mathbf{q}$ are found as follows, by considering the modal-space equivalent of Eq. (24):

$$\begin{bmatrix} \mathbf{q}_{\cos}^{(k)} \\ \mathbf{q}_{\sin}^{(k)} \end{bmatrix} = \begin{bmatrix} (\mathbf{\Lambda} - k^2\varpi^2\mathbf{I})^{-1} & \mathbf{0} \\ \mathbf{0} & (\mathbf{\Lambda} - k^2\varpi^2\mathbf{I})^{-1} \end{bmatrix} \left\{ \begin{bmatrix} \mathbf{H}_{\mathbf{v}}^{\mathrm{T}}\boldsymbol{\rho}_{\cos}^{(k)} \\ \mathbf{H}_{\mathbf{v}}^{\mathrm{T}}\boldsymbol{\rho}_{\sin}^{(k)} \end{bmatrix} + \begin{bmatrix} \mathbf{H}_{\mathbf{g}}^{\mathrm{T}}\mathbf{g}_{\cos}^{(k)} \\ \mathbf{H}_{\mathbf{g}}^{\mathrm{T}}\mathbf{g}_{\sin}^{(k)} \end{bmatrix} + \sum_{j=1}^{J} \delta_{k\varpi,\Omega_{(j)}} \begin{bmatrix} \mathbf{H}_{\mathbf{u}_{(j)}}^{\mathrm{T}}\mathbf{u}_{(j)\cos} \\ \mathbf{H}_{\mathbf{u}_{(j)}}^{\mathrm{T}}\mathbf{u}_{(j)\sin} \end{bmatrix} \right\}, \tag{37}$$

where

$$\mathbf{\Lambda} = \mathbf{diag}\{\omega_1^2, \ldots, \omega_R^2\}. \tag{38}$$

With reference to Eq. (30), the components $\bar{\tilde{\mathbf{q}}}$ were found as part of the solution process of the previous section. As for the non-rigid components $\tilde{\bar{\mathbf{q}}}$ in Eq. (30), these are given by the equation:

$$\tilde{\bar{\mathbf{q}}} = \tilde{\mathbf{\Lambda}}^{-1}\{\tilde{\mathbf{H}}_{\mathbf{v}}^{\mathrm{T}}\bar{\boldsymbol{\rho}} + \tilde{\mathbf{H}}_{\mathbf{w}}^{\mathrm{T}}\mathbf{w}\}, \tag{39}$$

where

$$\tilde{\mathbf{\Lambda}} = \mathbf{diag}\{\omega_{P+1}^2, \ldots, \omega_R^2\}, \tag{40a}$$

$$\tilde{\mathbf{H}}_{\mathbf{v}} = [\boldsymbol{\psi}_{\mathbf{v}}^{(P+1)} \ldots \boldsymbol{\psi}_{\mathbf{v}}^{(R)}], \tag{40b}$$

$$\tilde{\mathbf{H}}_{\mathbf{w}} = [\boldsymbol{\psi}_{\mathbf{w}}^{(P+1)} \ \ldots \boldsymbol{\psi}_{\mathbf{w}}^{(R)}]. \tag{40c}$$

### 2.6. Some observations

It is to be noted that concentrated viscous damping forces can be dealt with in a similar manner to the gyroscopic effect in Section 2.2. Distributed damping of the proportional type [9] in the linear part can also be accommodated into the above analysis. In this case, the receptance matrix expressions in Eqs. (19) are simply modified by changing their denominator to $\omega_r^2 - \omega^2 + \mathrm{j}2\zeta_r\omega\omega_r$, where $\mathrm{j} = \sqrt{-1}$ and $\zeta_r$ is the modal damping ratio [9]. Hence, in the first term of the right-hand side of Eq. (18), the matrices $\mathbf{C_{vv}}$ are replaced by $\mathrm{Re}\{\mathbf{C_{vv}}\}$ and the off-diagonal zero matrices are replaced by $\mathrm{Im}\{\mathbf{C_{vv}}\}$, $-\mathrm{Im}\{\mathbf{C_{vv}}\}$—similarly for the other terms.

Stability analysis is not performed here since available techniques [4,6] are not useful for systems with a large number of modes. However, a spot check can be performed at an arbitrary solution point on a speed response by running a time-marching analysis from initial conditions on the particular RHBM solution that is being tested: if the trajectory remains on the RHBM orbit then it is stable [6]. The initial state variables $\mathbf{q}(t=0)$, $\dot{\mathbf{q}}(t=0)$ are obtained through Eqs. (29) and Eqs. (37, 39).

## 3. Simulations

The RHBM was applied to a representative twin-spool aero-engine having the schematic layout in Fig. 1, using a realistically sized whole-engine FE model provided by an engine manufacturer. This engine-model was also used in Ref. [1] to test the IRM. In this section, the RHBM results for both SFU and MFU response are validated against the corresponding IRM results. All simulations were performed in Matlab on a standard 2006—issue desktop pc with Intel® Pentium® D CPU 3 GHz processor.

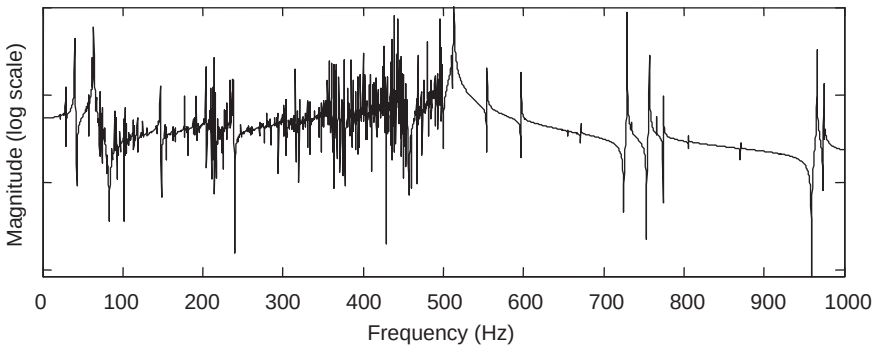


Fig. 4. Point receptance frequency response at point $B_1$ in $y$ direction [1].

Table 1
Test cases for RHBM.

| Case | Low pressure (LP) rotor | | | High pressure (HP) rotor | | |
|---|---|---|---|---|---|---|
| | $U_{(1)1}$ (kg mm) | $U_{(1)2}$ (kg mm) | $\gamma_{(1)2}$ | $U_{(2)1}$ (kg mm) | $U_{(2)2}$ (kg mm) | $\gamma_{(2)2}$ |
| A: SFU | 6.3 | 6.3 | 0 | 0 | 0 | 0 |
| B: MFU | 6.3 | 6.3 | 0 | 5.0 | 5.0 | 0 |

### 3.1. Linear pre-processing

As indicated in Fig. 2, a one-off eigenvalue analysis was performed on the linear part under non-rotational conditions. The results of the eigenvalue analysis were used during the course of the subsequent RHBM process to compute the required receptance matrices (Eqs. (19) and (21)). By way of illustration of a typical receptance function, Fig. 4 is reproduced from Ref. [1]. All 934 modes over the frequency range 0–1 kHz were included in the subsequent RHBM analysis due to the high shaft speeds and harmonics in the response. As observed in Ref. [1], the sudden reduction in modal density beyond 500 Hz is merely an artefact of the degree-of-freedom reduction technique used by the FE modellers.

### 3.2. Nonlinear computation for the unbalance response

The RHBM was tested for two cases A and B involving SFU and MFU, respectively, as illustrated in Table 1. In case A the unbalance was restricted to the LP rotor only. For each rotor the unbalance was concentrated at two locations. Fig. 5 indicates the positions of these locations, as well as the locations of the SFDs and the distribution of the weights of the two rotors. The gyroscopic effect was discretised at 7 points on the LP rotor and 12 points on the high-pressure (HP) rotor. For each cases A, B and RHBM speed response curves were computed for a fixed ratio $\Omega_{(2)}/\Omega_{(1)} = 1.2$ where $\Omega_{(1)}$, $\Omega_{(2)}$ are the LP, HP speeds, respectively. It should be mentioned that MFU results are affected by the angular position $\phi_{(2)}$ of the HP rotor relative to the LP rotor at the reference time $t = 0$. For the MFU results presented here $\phi_{(2)} = 0$. The influence of this parameter on the predicted MFU response will be investigated in a separate research work.

For these preliminary calculations, the bearing housings were assumed to be perfectly aligned with each other prior to rotor assembly (i.e. $\mathbf{v_s} = \mathbf{0}$ in Eq. (34)). As in Ref. [1], the SFDs considered for this study were single-land and end-fed with oil of viscosity $0.0049\,\mathrm{N\,s\,m^{-2}}$ at a pressure of 3 bar (gauge). The bearing diameters and radial clearances were typically 200 and 0.1 mm, respectively, and the land lengths ranged from 16 to 34 mm. Each iteration of the RHBM solution process required the evaluation of the Fourier coefficients of the SFD forces. As indicated in Fig. 3 this necessitated the generation of an $n_F$—point time history of the forces $\boldsymbol{\rho}_i(\mathbf{v}_i, \dot{\mathbf{v}}_i)$ at each SFD (where $n_F$ is a suitable number of points [6]). For each of these points, the forces at SFD no. $i$ were evaluated by numerical integration of the pressure distribution across the oil film at the

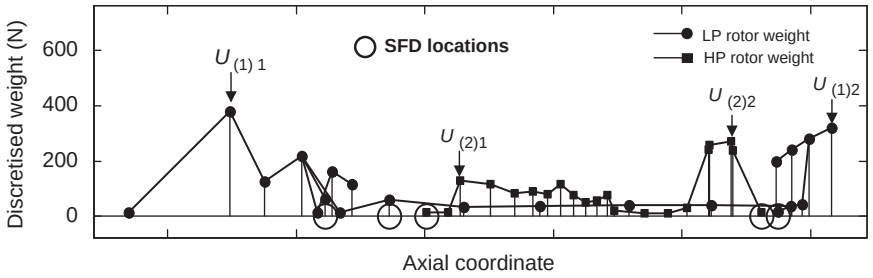


Fig. 5. Unbalance locations, bearing locations and rotor weight distribution.

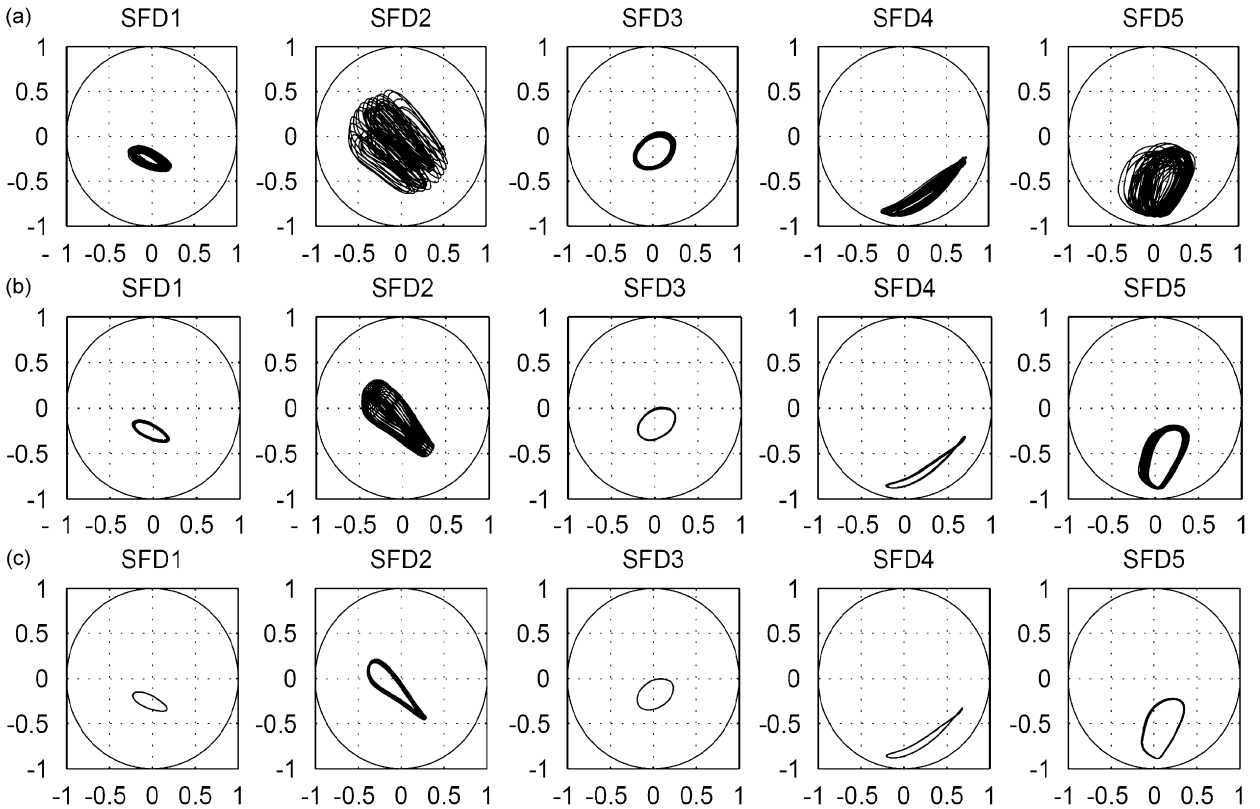


Fig. 6. Periodic steady-state solution obtained using a time-domain approach (IRM): (a) last 50 out of first 100 revolutions; (b) last 50 out of first 1000 revolutions; and (c) last 50 out of first 3000 revolutions (orbits normalised with respect to corresponding radial clearances).

instantaneous dynamic condition $\mathbf{v}_i, \dot{\mathbf{v}}_i$, as described in Ref. [1]. An "end-leakage factor" $\lambda = 0.03$ was used to account for the sealing at the ends of the dampers [1].

### 3.2.1. Case A: SFU

In this case, $\Omega_{(j_{\text{ref}})} = \Omega_{(1)}$ in Eq. (1) since the LP rotor carried the unbalance. A speed response curve was constructed for $Q = 1$ in Eq. (1) and $\Omega_{(2)}/\Omega_{(1)} = 1.2$. Eight harmonics of the fundamental frequency $\Omega_{(1)}$ were used (i.e. $K = 8$). The number of unknowns for each solution point was therefore 174 (including the $P = 4$ extra unknowns). With reference to the iterative process described in Fig. 3, $n_F = 19$ was adequate for the SFU computations described.

The first solution point on the speed response corresponded to LP, HP rotor speeds of 10,000 and 12,000 rev/min, respectively. For this first point (*only*), the initial approximation was provided by the Fourier

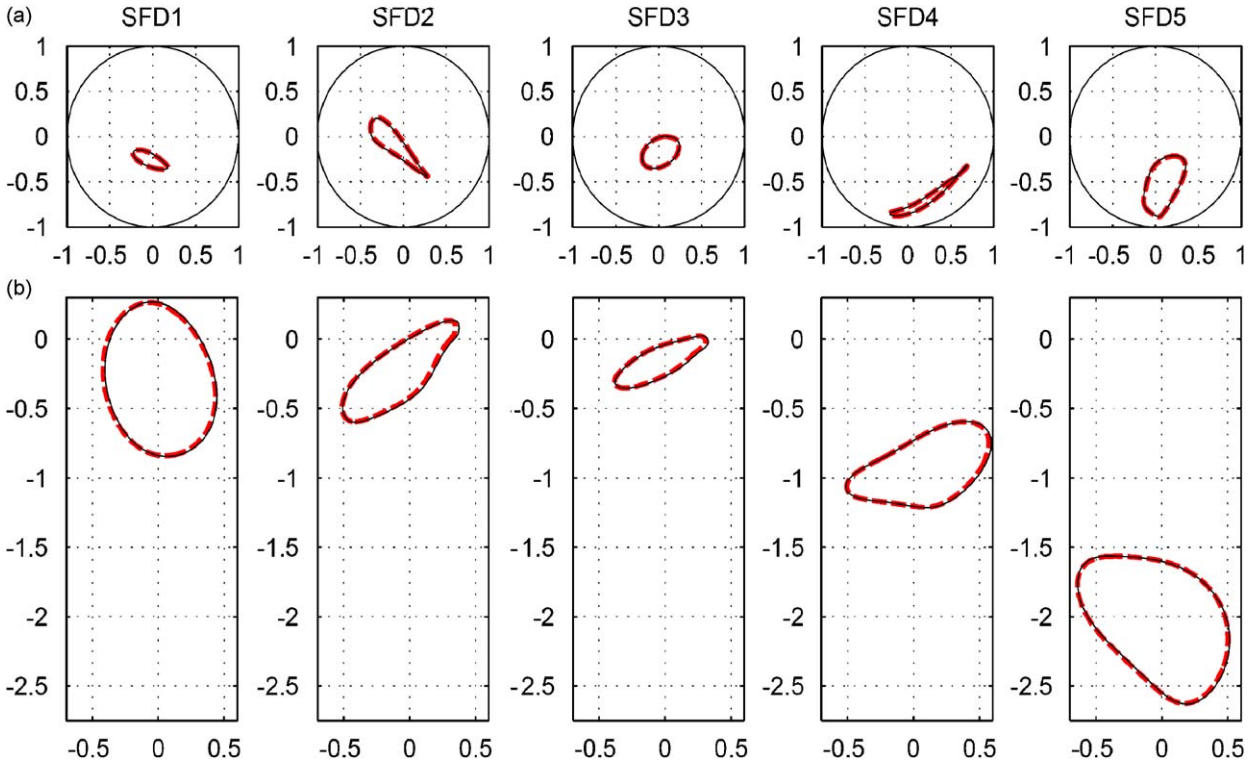


Fig. 7. Validation of RHBM (—) against steady-state IRM (- - -) for the starting solution of the SFU response curve: (a) orbits of the bearing journals within the radial clearance circles and (b) absolute displacement of the bearing-housing centres (orbits normalised with respect to the respective radial clearances).

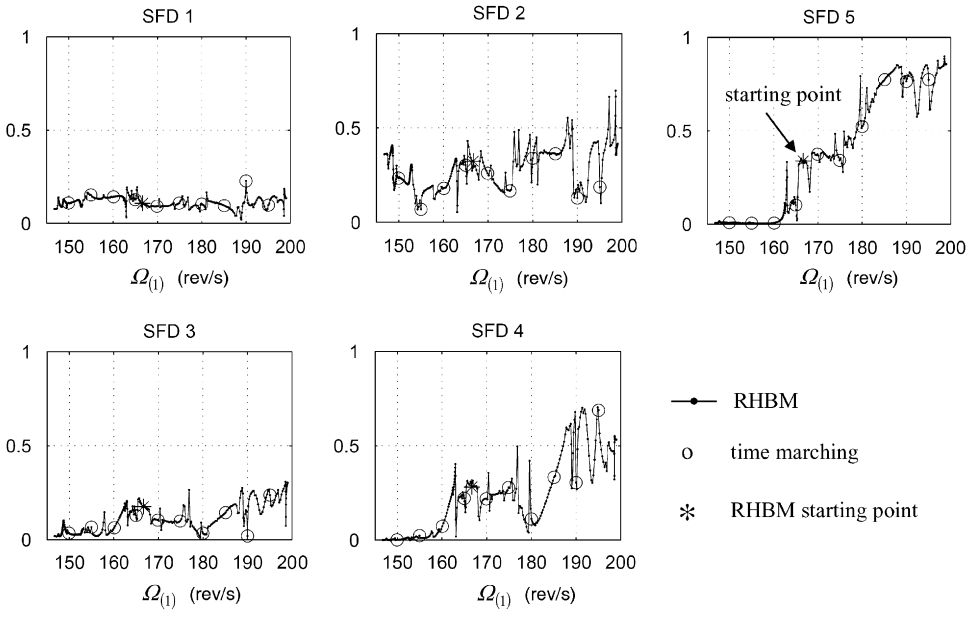


Fig. 8. SFU speed response curves of $y$ relative displacements at SFDs (vertical axes give half peak–peak amplitude normalised by radial clearance).

coefficients of the transient time domain solution obtained by the IRM [1]. Fig. 6 shows the IRM solution over 3000 LP shaft revolutions starting from initial conditions corresponding to zero relative displacements and velocities at each SFD. It is evident that the system dynamics dictated that a time-march through a very large number of revolutions (up to 4000) was necessary to reach complete steady-state (regardless of the type of time domain solver used). However, for the purpose of generating the RHBM approximation, the solution over the first 100 LP shaft revolutions (i.e. Fig. 6a) was sufficient: this took about 20 min to generate. Using this transient approximation, the RHBM took 5 s to converge to the steady-state periodic solution shown in Fig. 7. It is also noted that the RHBM also converged successfully in around the same time using a transient approximation generated in considerably less than 20 min by using cruder numerical accuracy (tolerance) settings for the IRM solver. Fig. 7 shows the excellent agreement between the RHBM and the steady-state IRM solution. This figure also shows the absolute vibration of the bearing housings which, in the case of RHBM, was recovered by the method described in Section 2.5.

Having generated this first RHBM solution point, a speed response curve was constructed as described in Section 2.4. This is expressed in Fig. 8 as a set of graphs showing the variation with LP shaft speed of the half-peak-to-peak amplitude of the relative $y$ displacement at each SFD. The steady-state IRM results at discrete speeds are overlaid on the same axes and show excellent correlation with the RHBM.

### 3.2.2. Case B: MFU

In this case, $\Omega_{(j_{ref})} = \Omega_{(1)}$ in Eq. (1) since it is the slower shaft. Since $\Omega_{(2)}/\Omega_{(1)} = 1.2 = 6/5$, the value of $Q$ in Eq. (1) was taken to be 5. Thirty-three harmonics of the fundamental frequency $\Omega_{(1)}/5$ were used (i.e. $K = 33$),

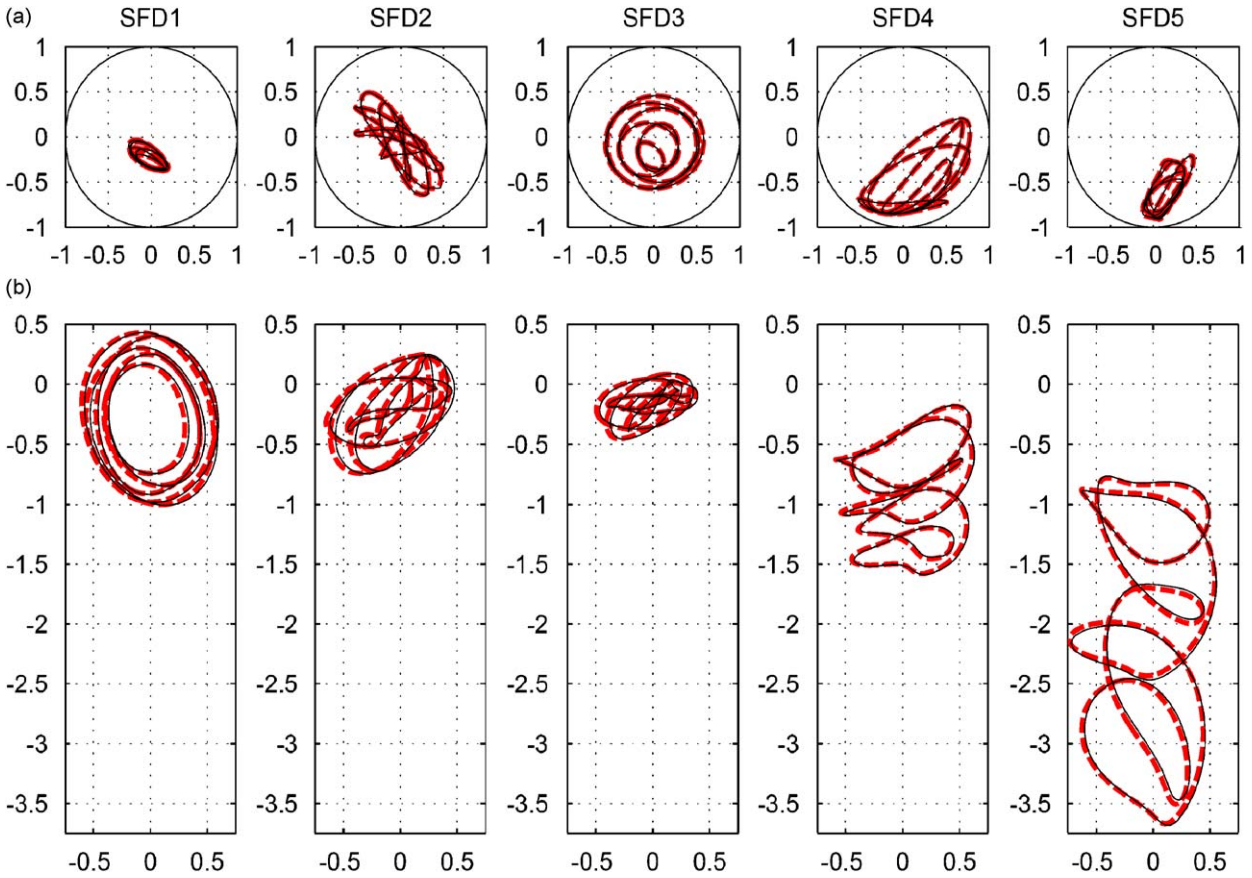


Fig. 9. Validation of RHBM (—) against steady-state IRM (- - -) for the starting solution of the MFU response curve: (a) orbits of the bearing journals within the radial clearance circles and (b) absolute displacement of the bearing-housing centres (orbits normalised with respect to the respective radial clearances).

resulting in 674 unknowns for each solution point. With reference to the iterative process described in Fig. 3, the value of $n_F$ had to be increased to 69.

As for the SFU case, the first solution point on the speed response corresponded to LP, HP rotor speeds of 10,000 and 12,000 rev/min, respectively. The initial approximation to this point was again provided by the Fourier coefficients of the transient IRM solution over the first 100 LP shaft revolutions. This approximation took roughly 20 min to produce and, using this, the RHBM took 50 s to converge to the steady-state periodic solution shown in Fig. 9. This figure shows the excellent agreement between the RHBM solution and the steady-state IRM solution (achieved after a total of 4000 LP shaft revolutions).

From this first RHBM solution point, the speed response curve of RHBM solutions depicted in Fig. 10 was generated. Excellent correlation is again seen between the RHBM and the discrete IRM results plotted in Fig. 10.

### 3.2.3. Discussion

It is to be noted that, as indicated in Fig. 1, SFDs 1 and 3 were spring-supported and the orbit offsets within the clearances of these SFDs were mainly due to the respective rotor weights (see Fig. 7a). The rest of the SFDs, particularly SFDs 4 and 5, relied on the relative vibration (between their journal and housing) to generate a lifted mean position within their clearances. Hence, it is the prediction of the response at these unsupported SFDs that posed the major computational challenge for the iterative process, particularly in the presence of a large number of harmonics.

Fig. 11 shows the development of the harmonic content of the RHBM SFU speed response at one of the unsupported SFDs. This figure refers to the relative $y$ displacement (mean removed) and velocity, the latter being included since the SFD force is a function of both relative displacement and velocity. This spectrum simply features the LP-synchronous frequency (“1LP”) and its harmonics: the HP-synchronous frequency is absent since there is no HP unbalance. It is also evident that an adequate number of harmonics has to be retained due to their prominence in the velocity spectrum.

Fig. 12 shows the development of the harmonic content of the RHBM MFU speed response at one of the unsupported SFDs. This spectrum features both LP- and HP-synchronous components, along with non-synchronous frequencies which are multiples of $\Omega_{(1)}/5$. It is evident that the sub-synchronous harmonics are

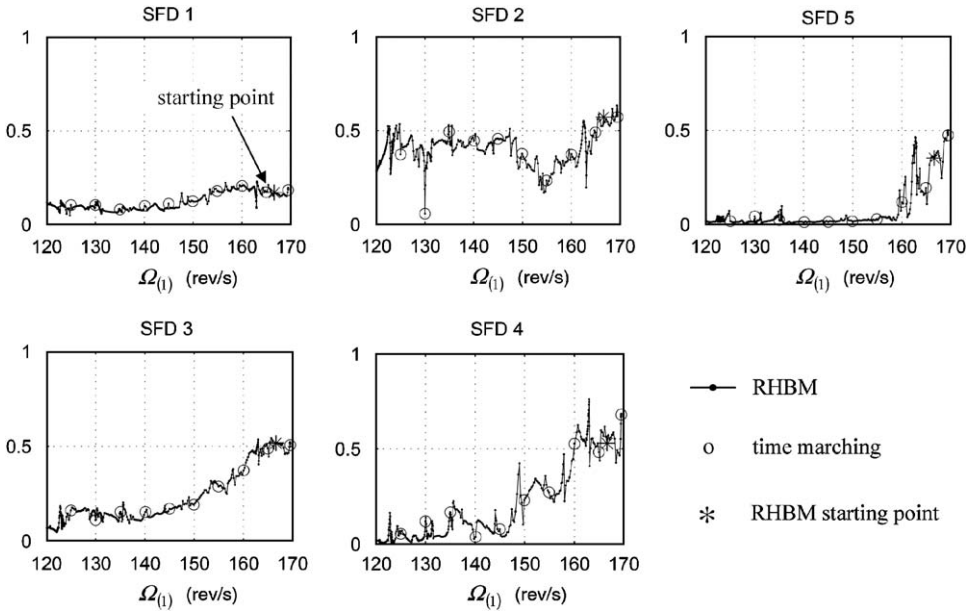


Fig. 10. MFU speed response curves of $y$ relative displacements at SFDs (vertical axes give half peak–peak amplitude normalised by radial clearance).

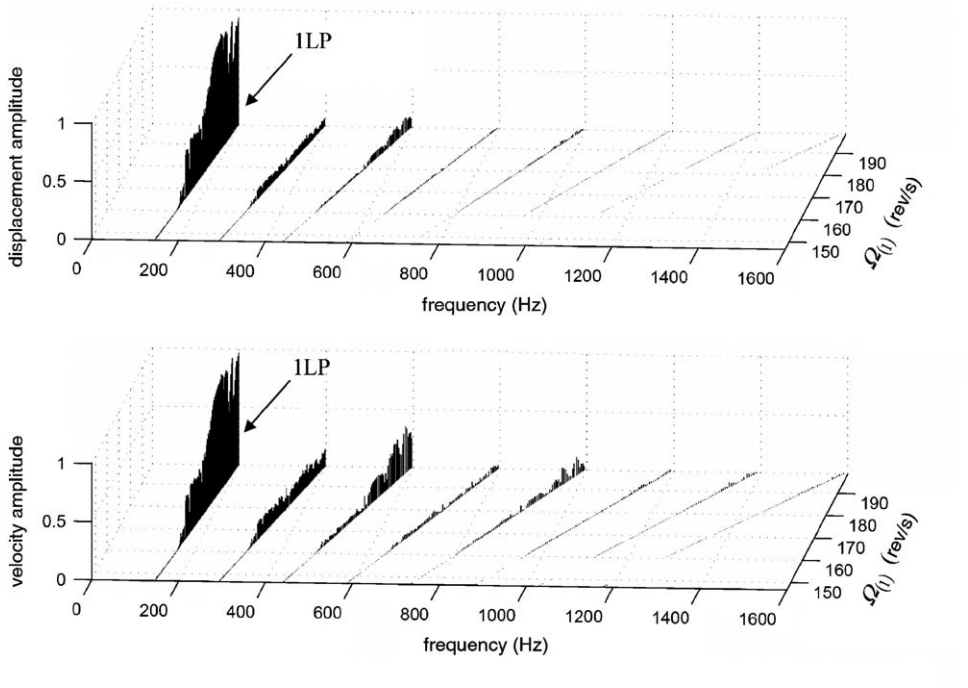


Fig. 11. Development of harmonics in RHBM SFU response at an unsupported SFD (harmonic amplitudes normalised with respect to greatest amplitude in the respective diagram).

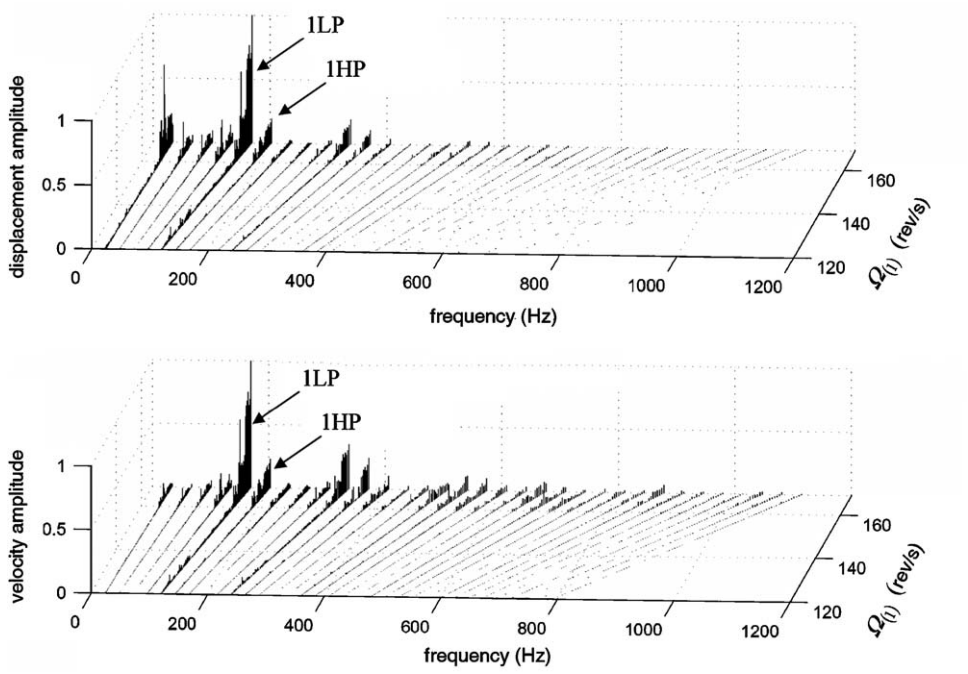


Fig. 12. Development of harmonics in RHBM MFU response at an unsupported SFD (harmonic amplitudes normalised with respect to greatest amplitude in the respective diagram).

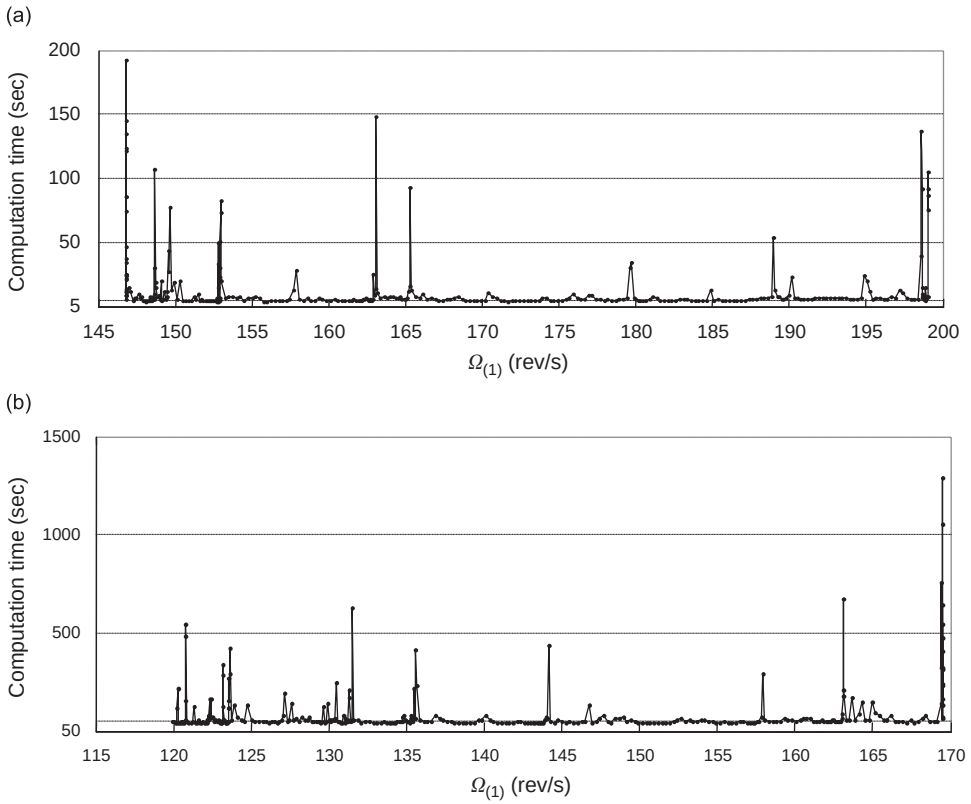


Fig. 13. Point-to-point computation time in generating the RHBM speed response curves using a rudimentary speed-control continuation process: (a) case A: SFU and (b) case B: MFU.

prominent in the relative displacement signals whereas the super-synchronous signals are prominent in the relative velocity signals.

Fig. 13 shows the variation of the computation time per solution point for both SFU and MFU speed response curves. The typical solution times per point for the two cases were 5 and 50 s, respectively. The total (cumulative) times to generate the speed response curve for the two cases were 85 and 550 min, respectively. However, these total times can be significantly cut through improvement of the algorithms used for the continuation procedure. Such numerical issues are outside the scope of this paper. Suffice to say that the continuation procedure used here was a rudimentary one in which the LP-speed was the control parameter and the solution at a prescribed speed-step was solved using the solution at the previous step as the predictor. When the iteration showed signs of divergence, it automatically restarted with a reduced step-size as many times as necessary until the solution converged. The spikes in Fig. 13 indicate that a large portion of the total time was taken up by a few very narrow regions where the process struggled to advance the solution. It is likely that a switch to arc-length continuation [6] in these regions would significantly reduce the number of failed attempts, thereby cutting the total computation time.

Finally, it should be emphasised that the RHBM is highly useful even in the absence of a continuation procedure. As illustrated in Section 3.2.1, "unfinished" time-domain solutions at a number of discrete speeds, each generated with crude tolerance settings over a small number of revolutions can each be "finished off" and refined to steady-state in a matter of seconds using the RHBM. This of course is conditional on the time-domain solution being indeed periodic in the steady-state, as in all the results presented here. As observed in Ref. [1], reducing the degree of sealing from $\lambda = 0.03$ (as used in the present paper) to a very low level ($\lambda = 0.01$), all other parameters being kept the same, resulted in a steady-state quasi-periodic response which could only be computed by a time-domain technique, as discussed in the Introduction.

## 4. Conclusions

In this paper, a whole-engine RHBM has been devised that, for the first time, has allowed the frequency domain computation of the steady-state periodic unbalance vibration of a whole aero-engine model with nonlinear bearings. The method uses the receptance functions of the linear part of the structure under non-rotational conditions, obtained from a one-off eigenvalue analysis, to set up the equations for the rotating nonlinear assembly. The unknowns solved for are the Fourier coefficients of the relative displacements at the nonlinear bearings plus a few extra unknowns. These latter unknowns enable solution of the problem in the presence of statically indeterminate rotors that have just one linear point support or none at all. Simulation tests were performed on a realistically sized representative twin-spool engine with rotors running at different speeds for both SFU (unbalance distribution confined to one rotor) and MFU (unbalance on both rotors). In either case, excellent correlation with time-marching results was obtained. For the cases studied, the computation time for MFU was about 10 times greater than SFU due to the larger number of harmonics necessary to describe the solution. However, for either case, it has been demonstrated that, when used in conjunction with a time-marching solver like the recently developed IRM, the RHBM is a very powerful tool that should greatly facilitate the hitherto highly restricted nonlinear dynamic analysis of realistic engine structures.

## Acknowledgements

The authors acknowledge the support of the EPSRC of the UK and the support of Rolls-Royce plc.

## Appendix A. Assembly of the matrices $\partial\bar{\boldsymbol{\rho}}/\partial\mathbf{z}$, $\partial\boldsymbol{\rho}_{\cos}^{(k)}/\partial\mathbf{z}$, $\partial\boldsymbol{\rho}_{\sin}^{(k)}/\partial\mathbf{z}$

For each SFD no. $i$, $i = 1 \ldots N$, calculate the partial derivatives:

$$\frac{\partial}{\partial\bar{\mathbf{v}}_i}\begin{bmatrix}\bar{\boldsymbol{\rho}}_i\\ \boldsymbol{\rho}_{i\,\cos}^{(1)}\\ \boldsymbol{\rho}_{i\,\sin}^{(1)}\\ \vdots\\ \boldsymbol{\rho}_{i\,\cos}^{(K)}\\ \boldsymbol{\rho}_{i\,\sin}^{(K)}\end{bmatrix},\quad \frac{\partial}{\partial\mathbf{v}_{i\,\cos}^{(k)}}\begin{bmatrix}\bar{\boldsymbol{\rho}}_i\\ \boldsymbol{\rho}_{i\,\cos}^{(1)}\\ \boldsymbol{\rho}_{i\,\sin}^{(1)}\\ \vdots\\ \boldsymbol{\rho}_{i\,\cos}^{(K)}\\ \boldsymbol{\rho}_{i\,\sin}^{(K)}\end{bmatrix},\quad \frac{\partial}{\partial\mathbf{v}_{i\,\sin}^{(k)}}\begin{bmatrix}\bar{\boldsymbol{\rho}}_i\\ \boldsymbol{\rho}_{i\,\cos}^{(1)}\\ \boldsymbol{\rho}_{i\,\sin}^{(1)}\\ \vdots\\ \boldsymbol{\rho}_{i\,\cos}^{(K)}\\ \boldsymbol{\rho}_{i\,\sin}^{(K)}\end{bmatrix},\quad k = 1 \ldots K. \tag{41}$$

Now

$$\frac{\partial\bar{\boldsymbol{\rho}}}{\partial\mathbf{z}} = \left[\mathbf{0}_{2N\times n_{\text{extra}}}\ \ \frac{\partial\bar{\boldsymbol{\rho}}}{\partial\bar{\mathbf{v}}}\ \ \frac{\partial\bar{\boldsymbol{\rho}}}{\partial\mathbf{v}_{\cos}^{(1)}}\ \ \frac{\partial\bar{\boldsymbol{\rho}}}{\partial\mathbf{v}_{\sin}^{(1)}}\ \cdots\ \frac{\partial\bar{\boldsymbol{\rho}}}{\partial\mathbf{v}_{\cos}^{(K)}}\ \ \frac{\partial\bar{\boldsymbol{\rho}}}{\partial\mathbf{v}_{\sin}^{(K)}}\right], \tag{42}$$

where

$$\frac{\partial\bar{\boldsymbol{\rho}}}{\partial\bar{\mathbf{v}}} = \mathbf{blkdiag}\left\{\frac{\partial\bar{\boldsymbol{\rho}}_1}{\partial\bar{\mathbf{v}}_1},\ldots,\frac{\partial\bar{\boldsymbol{\rho}}_N}{\partial\bar{\mathbf{v}}_N}\right\}, \tag{43a}$$

$$\frac{\partial\bar{\boldsymbol{\rho}}}{\partial\mathbf{v}_{\cos}^{(m)}} = \mathbf{blkdiag}\left\{\frac{\partial\bar{\boldsymbol{\rho}}_1}{\partial\mathbf{v}_{1\,\cos}^{(m)}},\ldots,\frac{\partial\bar{\boldsymbol{\rho}}_N}{\partial\mathbf{v}_{N\,\cos}^{(m)}}\right\}, \tag{43b}$$

$$\frac{\partial\bar{\boldsymbol{\rho}}}{\partial\mathbf{v}_{\sin}^{(m)}} = \mathbf{blkdiag}\left\{\frac{\partial\bar{\boldsymbol{\rho}}_1}{\partial\mathbf{v}_{1\,\sin}^{(m)}},\ldots,\frac{\partial\bar{\boldsymbol{\rho}}_N}{\partial\mathbf{v}_{N\,\sin}^{(m)}}\right\},\quad m = 1 \ldots K. \tag{43c}$$

For $k = 1 \ldots K$:

$$\frac{\partial \boldsymbol{\rho}_{\cos}^{(k)}}{\partial \mathbf{z}} = \left[ \mathbf{0}_{2N \times n_{\text{extra}}} \quad \frac{\partial \boldsymbol{\rho}_{\cos}^{(k)}}{\partial \bar{\mathbf{v}}} \quad \frac{\partial \boldsymbol{\rho}_{\cos}^{(k)}}{\partial \mathbf{v}_{\cos}^{(1)}} \quad \frac{\partial \boldsymbol{\rho}_{\cos}^{(k)}}{\partial \mathbf{v}_{\sin}^{(1)}} \cdots \frac{\partial \boldsymbol{\rho}_{\cos}^{(k)}}{\partial \mathbf{v}_{\cos}^{(K)}} \quad \frac{\partial \boldsymbol{\rho}_{\cos}^{(k)}}{\partial \mathbf{v}_{\sin}^{(K)}} \right], \tag{44}$$

where for each $k$:

$$\frac{\partial \boldsymbol{\rho}_{\cos}^{(k)}}{\partial \bar{\mathbf{v}}} = \mathbf{blkdiag}\left\{ \frac{\partial \boldsymbol{\rho}_{1\ \cos}^{(k)}}{\partial \bar{\mathbf{v}}_1}, \ldots, \frac{\partial \boldsymbol{\rho}_{N\ \cos}^{(k)}}{\partial \bar{\mathbf{v}}_N} \right\}, \tag{45a}$$

$$\frac{\partial \boldsymbol{\rho}_{\cos}^{(k)}}{\partial \mathbf{v}_{\cos}^{(m)}} = \mathbf{blkdiag}\left\{ \frac{\partial \boldsymbol{\rho}_{1\ \cos}^{(k)}}{\partial \mathbf{v}_{1\ \cos}^{(m)}}, \ldots, \frac{\partial \boldsymbol{\rho}_{N\ \cos}^{(k)}}{\partial \mathbf{v}_{N\cos}^{(m)}} \right\}, \tag{45b}$$

$$\frac{\partial \boldsymbol{\rho}_{\cos}^{(k)}}{\partial \mathbf{v}_{\sin}^{(m)}} = \mathbf{blkdiag}\left\{ \frac{\partial \boldsymbol{\rho}_{1\cos}^{(k)}}{\partial \mathbf{v}_{1\sin}^{(m)}}, \ldots, \frac{\partial \boldsymbol{\rho}_{N\cos}^{(k)}}{\partial \mathbf{v}_{N\ \sin}^{(m)}} \right\}, \quad m = 1 \ldots K. \tag{45c}$$

For $\partial \boldsymbol{\rho}_{\sin}^{(k)} / \partial \mathbf{z}$, replace the subscript "cos" by "sin" in the *numerators* of the partial derivative expressions of Eqs. (44) and (45).

## References


[1] P.M. Hai, P. Bonello, An impulsive receptance technique for the time domain computation of the vibration of a whole aero-engine model with nonlinear bearings, *Journal of Sound and Vibration* 318 (3) (2008) 592–605.

[2] A. Liew, N.S. Feng, E.J. Hahn, Application of transfer matrices to non-linear rotor-bearing systems, *Proceedings of ASME Design Engineering Technical Conference*: *17th Biennial Conference on Mechanical Vibration and Noise*, Las Vegas, 12–15 September 1999, Paper no. DETC99/VIB-8263, 9pp.

[3] E.J. Hahn, P.Y.P. Chen, Harmonic balance analysis of general squeeze film damped multidegree-of-freedom rotor bearing systems, *ASME Journal of Tribology* 116 (1994) 499–507.

[4] C.S. Zhu, D.A. Robb, D.J. Ewins, Analysis of the multiple-solution response of a flexible rotor supported on non-linear squeeze-film dampers, *Journal of Sound and Vibration* 252 (3) (2002) 389–408.

[5] C. Nataraj, H.D. Nelson, Periodic solutions in rotor dynamic systems with nonlinear supports: a general approach, *ASME Journal of Vibration, Acoustics, Stress, and Reliability in Design* 111 (1989) 187–193.

[6] P. Bonello, M.J. Brennan, R. Holmes, Non-linear modelling of rotor dynamic systems with squeeze film dampers—an efficient integrated approach, *Journal of Sound and Vibration* 249 (4) (2002) 743–773.

[7] P. Bonello, M.J. Brennan, R. Holmes, The prediction of the non-linear dynamics of a squeeze film damped aero-engine rotor housed in a flexible support structure, *Proceedings of the IMechE Part G Journal of Aerospace Engineering* 218 (3) (2004) 213–230.

[8] Y. Ren, C.F. Beards, A new receptance-based perturbative multi-harmonic balance method for the calculation of the steady-state response of non-linear systems, *Journal of Sound and Vibration* 172 (5) (1994) 593–604.

[9] D.J. Ewins, *Modal Testing: Theory and Practice*, Research Student Press, Letchworth, UK, 1984.

[10] G. Dahlquist, *Numerical Methods*, Prentice-Hall, Englewood Cliffs, NJ, 1974.